Zinc isotope composition of the Earth and its behaviour during planetary accretion

Paolo Sossi, Oliver Nebel, Hugh St.C. O'Neill, Frédéric Moynier

▶ **To cite this version:**

Paolo Sossi, Oliver Nebel, Hugh St.C. O'Neill, Frédéric Moynier. Zinc isotope composition of the Earth and its behaviour during planetary accretion. Chemical Geology, 2018, 477, pp.73-84. 10.1016/j.chemgeo.2017.12.006 . insu-02917173

HAL Id: insu-02917173

https://insu.hal.science/insu-02917173

Submitted on 19 Aug 2020

HAL is a multi-disciplinary open access archive for the deposit and dissemination of scientific research documents, whether they are published or not. The documents may come from teaching and research institutions in France or abroad, or from public or private research centers.

L'archive ouverte pluridisciplinaire **HAL**, est destinée au dépôt et à la diffusion de documents scientifiques de niveau recherche, publiés ou non, émanant des établissements d'enseignement et de recherche français ou étrangers, des laboratoires publics ou privés.

Accepted Manuscript

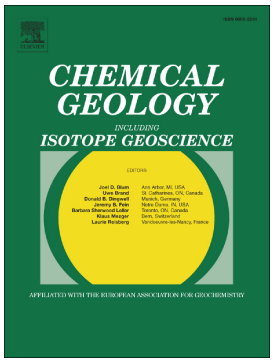

Zinc isotope composition of the Earth and its behaviour during planetary accretion

Paolo A. Sossi, Oliver Nebel, Hugh St.C. O'Neill, Frédéric Moynier

PII: S0009-2541(17)30678-2
DOI: https://doi.org/10.1016/j.chemgeo.2017.12.006
Reference: CHEMGE 18577

To appear in: *Chemical Geology*

Received date: 22 September 2017
Revised date: 6 December 2017
Accepted date: 8 December 2017

Please cite this article as: Paolo A. Sossi, Oliver Nebel, Hugh St.C. O'Neill, Frédéric Moynier , Zinc isotope composition of the Earth and its behaviour during planetary accretion. The address for the corresponding author was captured as affiliation for all authors. Please check if appropriate. Chemge(2017), https://doi.org/10.1016/j.chemgeo.2017.12.006

This is a PDF file of an unedited manuscript that has been accepted for publication. As a service to our customers we are providing this early version of the manuscript. The manuscript will undergo copyediting, typesetting, and review of the resulting proof before it is published in its final form. Please note that during the production process errors may be discovered which could affect the content, and all legal disclaimers that apply to the journal pertain.

ACCEPTED MANUSCRIPT

Zinc isotope composition of the Earth and its behaviour during planetary accretion

Paolo A. Sossi[1,2*], Oliver Nebel[3], Hugh St.C. O'Neill[1], Frédéric Moynier[2]

[1] Research School of Earth Sciences, Australian National University, Acton 2601, ACT, Australia

[2] Institut de Physique du Globe de Paris, Sorbonne Paris Cité, Université Paris Diderot, CNRS, F-75005 Paris, France

[3] School of Earth, Atmosphere and Environment, Monash University, Clayton 3800, VIC, Australia

*Corresponding author. Email address: sossi@ipgp.fr

Abstract

The terrestrial planets are depleted in volatile elements with respect to chondritic meteorites, their possible building blocks. However, the timing, extent and origin of volatile depletion is debated. Zinc is a moderately volatile element (MVE), whose stable isotopic composition can distinguish when and where this depletion took place. Here, we report data for 40 ultramafic rocks comprising pristine upper mantle peridotites from the Balmuccia orogenic lhezolite massif and Archean komatiites that together define the Zn isotope composition of the Earth's primitive mantle. Peridotites and komatiites are shown to have indistinguishable Zn isotopic compositions of $\delta^{66}Zn = +0.16 \pm 0.06$‰ (2SD), (with $\delta^{66}Zn$ the per mille deviation of $^{66}Zn/^{64}Zn$ from the JMC-Lyon standard), implying a constant Zn isotope composition for the silicate Earth since 3.5 Ga. After accounting for Zn sequestration during core formation, the Earth falls on the volatile-depleted end of a carbonaceous chondrite array, implying Earth avoided modification of its MVE budgets during late accretion (e.g., during a giant impact), in contrast to the Moon. The Moon deviates from the chondritic array in a manner consistent with evaporative loss of Zn, where its $\delta^{66}Zn$ co-varies with Mn/Na, implying post-nebular volatile loss is more pronounced on smaller bodies. Should the giant impact deliver the Earth's volatile complement of Pb and Ag, it cannot account for the budget of lithophile MVEs (*e.g.*, Zn, Rb, Mn), whose abundances reflect those of Earth's nebular building blocks. The Earth initially accreted from material that experienced chemical- and mass-dependent isotopic fractionation akin to carbonaceous chondrites, though volatile depletion was more pronounced on Earth.

Word count: 7504

Key Words: Zinc; Peridotite; Komatiite; Mantle; Nebula; Isotope

ACCEPTED MANUSCRIPT

1.0. Introduction

In comparison with the Sun and CI chondrites, the Bulk Silicate Earth (BSE) is depleted in moderately volatile elements (MVEs), normalised to the main constituents of the rocky planets, Fe, Mg and Si. Moderately volatile elements condense from a gas of solar composition at temperatures below those of the main constituents, assuming thermodynamic equilibrium and pressures of 10^{-4} bar (Lodders, 2003), and, are variably depleted in most chondrites compared to CI chondrites (Wasson and Kallemeyn, 1988). Since CI chondrites have elemental abundances, save for the most volatile, H, C, N, O and the noble gases, that match those of the Sun, they represent a default baseline from which the degree of volatile depletion may be quantified. This is achieved by normalising the abundance of a given MVE to a lithophile element that behaves in a nominally refractory manner (here, Mg), divided by the same ratio in CI chondrites, defining a depletion factor, $(MVE/Mg)/(MVE/Mg)_{CI}$. The pattern of MVE depletion in the Earth is different to that in any kind of meteorite, either chondritic or achondritic (O'Neill and Palme, 2008).

The dual siderophile and/or chalcophile character of many MVEs creates ambiguity as to whether MVE depletion in the terrestrial planets arose from core formation or volatility (Wood and Halliday, 2010; Ballhaus et al., 2013). Furthermore, this net depletion on Earth, as in other rocky planets, is the sum of two distinct processes: those responsible for MVE depletions in chondrites (nebular; *e.g.* Humayun and Cassen, 2000), upon which are superimposed volatile transfer mechanisms during the late stages of accretion (post-nebular; *e.g.* O'Neill and Palme, 2008). These post-nebular processes must occur at different thermodynamic conditions to those extant in the solar nebula, and thus give rise to elemental and isotopic fractionation that is not observed in chondrites. For example, the superchondritic Mn/Na ratios inferred for small telluric bodies (though notably not the Earth) likely reflect evaporation and loss of vapour under oxidising conditions (O'Neill and Palme, 2008). Moreover, the enrichment in the heavier Mg isotopes of the Earth (Hin et al., 2017) compared to most chondrites groups has been taken as empirical evidence for post-nebular volatile loss on Earth. Nevertheless, these processes remain poorly understood and thus conjecture abounds as to whether the Earth acquired its complement of volatile elements at an early (Halliday and Porcelli, 2001) or late stage (Schönbächler et al., 2010; Albarede et al., 2013) and whether chondritic meteorites are suitable analogues for its composition.

ACCEPTED MANUSCRIPT

The monovalent and lithophile element Zn, with its simple geochemistry during igneous differentiation, is an ideal element for detecting volatile delivery or loss during planetary accretion (Day and Moynier, 2014). The cosmochemical utility of Zn lies in its ability to track interactions between gaseous species and condensed phases (liquid/solid), by virtue of its low half-condensation temperature (T_C); 726 K (Lodders, 2003). Zinc isotope fractionation may arise from evaporation of condensed Zn hosted in silicates to Zn^0 (the stable gas phase; Lamoreaux et al., 1987), and is associated with mass-dependent, heavy isotope enrichment in the residue, be it at equilibrium or via kinetic processes. However, which end-member scenario characterises volatile loss during planetary formation, remains unconstrained, despite the fact that these processes may be distinguished by their stable isotope signatures. Namely, equilibrium isotope fractionation of Zn between condensed phase(s) and gas is smaller, especially at high temperatures (the $^{66}Zn/^{64}Zn$ fractionation factor between $ZnO_{(s)}$ and $Zn^0_{(g)}$ is $0.31‰ \times 10^6/T^2$; Ducher et al., 2016), than kinetically-driven vapour loss into a vacuum which is temperature-independent and scales with the inverse square root of the masses of the two evaporating isotopes (*cf.* Richter et al., 2002). The low Zn abundance of lunar mare basalts and highland rocks, coupled with their enriched $\delta^{66}Zn$ composition (≈1.4‰, Paniello et al., 2012; Kato et al., 2015) is consistent with evaporative loss, likely following degassing of a magma ocean or the Moon-forming giant impact. By contrast, the different classes of carbonaceous chondrites show only a small range in $\delta^{66}Zn$, ≈0.3‰, where $\delta^{66}Zn$ decreases with Zn/Mg, the opposite to that expected from volatilisation and is interpreted as reflecting two-component mixing in the solar nebula (Luck et al., 2005; Pringle et al., 2017). The position of Earth in the context of these reservoirs may serve in discerning when and where volatile depletion occurred.

Here, we present new Zn isotope data for terrestrial peridotites and komatiites. Combined, these data allow assessment of the primitive mantles Zn isotope composition, representative of the BSE. Accurate determination of these values is contingent upon selecting representative samples, since stable isotopes can fractionate during core formation, partial melting, and igneous differentiation. Therefore, we analysed fresh, unmetasomatised peridotite samples, from depleted dunites to fertile lherzolites and pyroxenites, from the orogenic massif Balmuccia, Italy (Hartmann and Wedepohl, 1993) emplaced in the lower crust prior to 285 Ma and likely at 453±35 Ma (Obermiller, 1994), representing contemporary upper mantle. These samples are complemented by komatiites sourced from four different cratons with ages ranging from 3.5-2.7 Ga, representing high-degree partial melts of mantle sourced from plumes (Sossi et al., 2016a). Together, they constrain the zinc isotope composition of the Earth's mantle

ACCEPTED MANUSCRIPT

through space and time, from 3.5 Ga to present. Allowing for the effect of core formation, the MVE history of Earth is contrasted against chondritic meteorites, which act as a suitable starting point to discern between nebular and post-nebular fractionation.

2.0. Samples

Peridotites from the Balmuccia Orogenic Lherzolite Massif, Ivrea Zone, NW Italy

Peridotitic and pyroxenitic ultramafic samples come from a single massif, the ≈4.5 km long, 0.5 km wide Balmuccia orogenic lherzolite (Shervais and Mukasa, 1991) affording a snapshot of mantle processes preserved in time. The suitability of these rocks for helping constrain the zinc isotope composition of the Earth's mantle also lies in their pristine nature. Lherzolites, which comprise the bulk of the massif, are fertile (≈13% clinopyroxene), fresh (negative loss-on-ignition) and unmetasomatised (Hartmann and Wedepohl, 1993). Petrographic descriptions, mineral chemistry and an overview of the tectonic history and geological setting of the samples used in this work can be found in Shervais and Mukasa (1991). Samples were collected at the same location as in the aforementioned studies, along the river that bisects the massif at its southern tip, and hence are directly comparable petrologically.

For this work, the samples are subdivided, based on their whole rock chemistry, as a) normal lherzolites (38.5 – 40.5 % MgO), b) depleted lherzolites (40.5 – 43.5 % MgO) and c) dunites (> 46 % MgO). Normal lherzolites are representative of the initial composition of the massif, and, with 39.3±0.5 wt% MgO and Mg# = 0.895, they are residues of 8±2 % fractional melting of a primitive mantle source of Palme and O'Neill (2014) (Sossi and O'Neill, in prep.). Progressive increase in MgO reflects a decrease in modal clinopyroxene, owing to partial fusion and its segregation into pyroxenite veins. Pyroxenites fall into two suites; the Chrome-Diopside and Aluminium-Augite types. The former are consistent with local mobilisation of clinopyroxene from the adjacent lherzolites, and therefore have similar petrological characteristics (e.g. Rivalenti et al., 1995). By contrast, the Al-Aug suite rocks are more evolved clinopyroxene-spinel crystal cumulates from a low-degree melt derived from a composition similar to the Balmuccia lherzolite. Dunites are often found adjacent to Chrome-Diopside pyroxenite segregations, and are residues of pyroxene removal and melt infiltration (Mazzucchelli et al., 2008).

Komatiites

The petrogenesis and geochemistry of the komatiites and komatiitic basalts in this work are described in Sossi et al. (2016a). A subset of these were analysed for their Zn isotope

ACCEPTED MANUSCRIPT

composition, and come from 4 separate cratons; the Kaapvaal (3), the Superior (3), the Zimbabwe (2), and the Pilbara (5), and comprise both Aluminium-Depleted and Aluminium-Undepleted komatiites (Nesbitt and Sun, 1979). Their eruptive ages range from 2.7 to 3.5 Ga, thereby representing not only a broad spatial, but a temporal cross-section of Archean magmatism. The samples are subdivided into petrological groups; the olivine cumulates (OCs), spinifex-textured komatiites (STKs), spinifex-textured basalts (STBs) and basalts (Bs). The spinifex-textured examples, owing to the quick cooling rates they experienced (Donaldson, 1976), closely approximate primary liquids.

3.0.Methods

An important consideration in ensuring the fidelity of isotope analyses of ultramafic rocks is their complete dissolution, which is hindered by the presence of refractory chromite. Despite its low modal abundance in komatiites (<5%), the budget of Zn in chromite is significant due to its higher partition coefficient ($D_{Zn}^{Min-Melt}$ = 5.2; Davis et al. 2013) relative to ferromagnesian silicates ($D_{Zn}^{Min-Melt} \leq 1$). The difficulty of spinel breakdown (nearer the magnesiochromite end member, $MgCr_2O_4$ in these compositions) is proportional to its Cr#. Although Cr_2O_3 is resistant to digestion in HNO_3-HCl-HF mixtures at ambient pressure and 130°C, its oxidised counterpart, Cr^{6+}, is readily soluble (*e.g.*, Sulcek and Povondra, 1989). To ensure quantitative digestion of chromite, 100 mg of powder was weighed in 3 mL Teflon beakers with concentrated HCl-HF-HNO_3 at 1:0.5:0.2 and left to dissolve at ≈130°C. After drying-down, concentrated HNO_3-HF (1:0.5) were added, and the samples placed inside 20 mL FEP Teflon vessels and inserted into steel bombs in an oven at ≈210°C for 7 days, sufficient to ensure complete dissolution of chromite.

Samples were then evaporated whilst 0.5 mL volumes of 15 M HNO_3 were added periodically to inhibit the formation of insoluble fluoride complexes. The samples were then dissolved in 6 M HCl, dried down, and re-dissolved again in 1 mL 6 M HCl in preparation for column chromatography. The samples were processed on 1 mL of AG1-X8 (200-400 mesh) anion exchange resin in BioRad ® PolyPrep columns (Sossi et al., 2015). Briefly, this involves sample loading and Cu elution in 6 M HCl, before iron is removed by adding 0.5 M HCl. Finally, Zn is eluted in 3 M HNO_3; only one pass through this column procedure was necessary to obtain purity sufficient for isotope analyses. The total Zn recovery is within uncertainty of 100%.

ACCEPTED MANUSCRIPT

After being evaporated completely as nitrates following addition of 15 M HNO_3, the samples were dissolved in 2 mL 2% (0.317 M) HNO_3 in readiness for mass spectrometric measurement. All solutions (samples and standards) were then diluted to 300 ppb, to which 300 ppb of Cu was added, to act as the external element for mass bias correction, as described in Sossi et al. (2015). Purified samples were run on a ThermoFinnigan Neptune Plus Multiple Collector Inductively-Coupled Plasma Mass Spectrometer (MC-ICP-MS) housed at the Research School of Earth Sciences, Australian National University and at the Institut de Physique du Globe de Paris (samples marked * in Table 1). Solutions were introduced via a glass nebuliser at 100 µL/min into a Scott Double Pass-Cyclonic Spray Chamber, before passing through standard cones (H skimmer; normal sampler) and low resolution slits. Under these conditions, typical sensitivities were 21 V/ppm ^{65}Cu and 10 V/ppm ^{64}Zn, and Ni and Ti signals, which can form oxide-based interferences on Zn masses, were checked for each sample and were lower than 10^{-3} V (^{62}Ni), yielding $^{64}Zn/^{64}Ni > 10000$, leading to corrections of <0.1‰ $\delta^{66}Zn$, and 10^{-2} V (^{48}Ti), the limit required to prevent any resolvable effect of the $^{48}Ti^{16}O$ polyatomic interference on ^{64}Zn (see Sossi et al., 2015). Each cycle consisted of a 1 s idle time of and an integration over the peak centre of 4.194 s, with forty per analysis. Under such conditions, the measurement repeatability was ± 0.02‰ (2SD) on the Ni-corrected $^{66}Zn/^{64}Zn$ ratio. Repeated running of standard rock powders through the entire procedure (dissolution, chromatography, mass spectrometry) reveal an external reproducibility of ±0.06‰ (2SD). Isotopic values are reported in delta notation relative to JMC-Lyon, $[(^{6x}Zn/^{64}Zn)_{sample}/(^{6x}Zn/^{64}Zn)_{JMC\text{-}Lyon}\text{-}1]*1000 = \delta^{6x}Zn$, where x = 6 or 8.

To ensure that the isotope data for the samples are accurate, three samples of known composition were run. The first, a pure solution standard (JMC-LMTG) was not processed through the columns, yielded a value of $\delta^{66}Zn$ = -0.09±0.05‰ (*n*, number of samples = 3) relative to the JMC-Lyon standard, in agreement with previously reported values (-0.11±0.05‰, *n* = 5; Sivry et al. 2008). In addition, the Allende CV3 chondrite, Hawaiian basalt BHVO-2 and serpentinised peridotite PCC-1 were also measured, yielding +0.21±0.04‰ (*n* = 2), +0.28±0.06‰ (*n* = 2) and +0.27±0.08‰ (*n* = 2), respectively. Recent determinations of the $\delta^{66}Zn$ of Allende (Pringle et al., 2017) yield 0.29±0.04‰, within uncertainty of the value reported here. It should be noted that some Calcium-Aluminium Rich Inclusions (CAIs), which comprise ~3% of Allende (Ebel et al. 2016) are enriched in the lighter isotopes of zinc (Luck et al., 2005; Kato and Moynier 2017) and may contribute to heterogeneity in the Zn isotope composition of Allende fragments. The BHVO-2 composition agrees with a compilation of 5

ACCEPTED MANUSCRIPT

independent measurements that yield +0.28±0.04‰ (Sossi et al., 2015). Although PCC-1 best matches the Mg-rich matrices of the samples measured herein, only one other reported value exists in the literature, +0.21±0.10‰ (Makishima and Nakamura, 2013) that overlaps with our determination. Uncertainties quoted in Table 1 and elsewhere are 2×standard deviations of replicate measurements on the MC-ICP-MS, and if not available, the total procedural uncertainty (±0.06‰ 2SD).

4.0. Results

Zinc isotope compositions of all samples, along with pertinent geochemical data, are reported in Table 1. The 19 peridotites have 31.79 < MgO (wt%) < 48.38, including eleven normal lherzolites (38 < MgO (wt%) < 42), with an average δ^{66}Zn=0.14±0.06‰ (Fig. 1a). The three depleted lherzolites and three dunites have indistinguishable averages of +0.13±0.05‰ and +0.14±0.06‰, indicating that all peridotitic lithologies in the massif are homogeneous with respect to zinc isotopes. This result, combined with the constancy of Zn contents (48±7 ppm; Table 1, Fig. 1b), despite marked changes in mineralogy, shows that zinc and its isotopes are evenly distributed throughout mantle phases, that is, $K_{D\,Zn}^{min/min} \approx 1$. The three pyroxenite samples (MgO ≈20 wt%), however, are marginally heavier, and average δ^{66}Zn = 0.21±0.04‰.

Magnesia in komatiitic rocks ranges from 43.69 wt% in olivine cumulate sample 331/788 to 4.05 wt% in sample 179/753, a differentiated basalt from the Coonterunah Subgroup (Fig. 1a). These two samples also define the minimum and maximum Zn contents s, between 22 to 178 ppm, respectively and 331/788 is the lightest sample with δ^{66}Zn = +0.04‰ and 331/778, a spinifex-textured basalt from the Komati formation the heaviest at +0.24‰, (Fig. 1b). Though none of the komatiite subgroups show a statistical difference from one another, a broad trend of increasing δ^{66}Zn with falling MgO is apparent, similar to that observed for a co-genetic sequence of rocks from Kilauea Iki, Hawai'i (Chen et al., 2013). However, the basaltic samples (+0.22±0.04‰, n = 5) with 13.84 to 4.05 wt% MgO, are marginally heavier than spinifex-textured komatiites (δ^{66}Zn = 0.18±0.04‰, n = 11).

The generally lighter isotope composition of ultramafic samples with respect to basalts is in accord with previously reported analyses of mantle peridotites. A marked contrast was found between fertile lherzolites from basalt-hosted off-craton peridotite xenoliths (δ^{66}Zn = 0.30±0.06‰, n = 11) and highly refractory kimberlite-hosted harzburgites with δ^{66}Zn = 0.14±0.06‰, n = 6 (Doucet et al., 2016). On the other hand, orogenic lherzolites from the North

ACCEPTED MANUSCRIPT

China Craton are relatively homogeneous in composition, $\delta^{66}Zn$ = 0.18±0.06‰, *n* = 25 (Wang et al., 2017) for a wide range of MgO and Zn contents, from 37.7 to 49.3 wt% and 58 to 35 ppm, respectively. This lack of isotopic variation is also recorded in the Balmuccia massif.

5.0.Discussion

5.1. Disturbance of Zn in ultramafic rocks

Petrographically, the peridotites of the Balmuccia massif are free of secondary alteration effects, indicated by the preservation of primary olivine and negative Loss-on-Ignition values (Hartmann and Wedepohl, 1993; Shervais and Mukasa, 1991). On the other hand, all Archean komatiites have experienced metamorphic retrogression by crustal fluids, which may have mobilised zinc.

The fidelity of Zn concentrations in a series of differentiating rocks may be determined through normalisation of Zn to another element that behaves conservatively and is geochemically similar. This role is fulfilled by Fe, whose high concentration in komatiites (≈11 wt. % FeO^T) and similar compatibility to that of Zn into olivine, near unity (e.g. Le Roux et al., 2010; Davis et al., 2013), render it an appropriate choice. Indeed, the observation that $K_{D(ol/melt)}^{Zn/Fe}$ = 0.92±0.07 (Le Roux et al., 2010) suggests that, if undisturbed, komatiitic rocks should lie on olivine control lines that produce near constant Zn/Fe ratios in evolving liquids. Samples that diverge markedly from constancy have therefore experienced secondary modification.

Here, a simple olivine fractional crystallisation/accumulation model is constructed in which the parental magma has 25 wt. % MgO, 11 wt. % $FeO^{(T)}$, an $Fe^{3+}/Fe^{(T)}$ of 0.10 and Zn content of 60. The $K_D^{Fe\text{-}Mg}$ exchange between olivine and melt is 0.30 (Toplis, 2005). The Zn/Fe evolution with MgO closely parallels that of the whole rocks (Fig. 2). Additionally, that the samples have Zn/Fe ratios very similar to that of the primitive mantle (Palme and O'Neill, 2014) and the Balmuccia peridotites substantiates not only that the trend is primary, but that the absolute values are, too. Samples plotting off the array are 179/753 and 179/755. Sample 179/753 is a differentiated basalt, hence it is not solely the product of olivine fractionation. Rather, Zn may have been enriched by crystallisation of Zn-poor minerals, plagioclase and pyroxene. This logic does not apply to sample 179/755, a spinifex-textured komatiite. Therefore, in this case, the Zn content appears to have been increased from its initial value. Despite this, its $\delta^{66}Zn$ is +0.20‰, consistent with the other STKs. It is concluded that the

ACCEPTED MANUSCRIPT

measured Zn isotope composition of metamorphosed Archean komatiites can be regarded as reflecting the primary signature of the magma from which they formed.

5.2. Principles of zinc isotope fractionation during magmatic differentiation

The two central processes that involve mass transfer in igneous petrogenesis, and are thus capable of fractionating Zn isotopes, are partial melting and fractional crystallisation. Given that olivine is the liquidus phase in mafic and ultramafic magmas above 8 wt% MgO (Kinzler and Grove, 1985) and constitutes ≈55 % of peridotites, coupled with the fact that Zn is distributed sub-equally between the two phases (*i.e.*, $D_{Zn}^{Ol-Melt} = 1$; Le Roux et al., 2010; Davis et al., 2013) olivine-melt equilibria must control Zn isotope fractionation, where Zn^{2+}, substitutes for Fe^{2+} and Mg^{2+} on the octahedral M-sites of olivine:

$$ZnO^{liq} + MgSi_{0.5}O_2{}^{ol} = MgO^{liq} + ZnSi_{0.5}O_2{}^{ol}. \quad (1)$$

As the activity of $MgSi_{0.5}O_2{}^{ol}$ varies little in ultramafic rocks (X_{Mg} = 0.9), the partitioning of zinc is dependent only on melt composition and temperature. The equilibrium constant for reaction (1) is:

$$K_{D\,Ol/Melt}^{Zn/Mg} = \left[\frac{X_{Zn}^{Ol}}{X_{Zn}^{Liq}}\right] / \left[\frac{X_{Mg}^{Ol}}{X_{Mg}^{Liq}}\right]. \quad (2)$$

The fact that $K_{D\,Ol/Melt}^{Zn/Mg} \approx 0.2 < K_{D\,Ol/Melt}^{Fe/Mg} \approx 0.3$ in basaltic melts (Kohn and Schofield, 1994) implies that Zn^{2+} is more incompatible and has a different co-ordination to Fe^{2+}, which is near V- to VI-fold in melts (Wilke, 2005). Owing to the full occupation of valence shell electrons (a $3d^{10}$ configuration), Zn^{2+} has no octahedral site preference energy and thus tends to form tetrahedral compounds (*e.g.,* Zn olivine, willemite, Zn_2SiO_4; Neumann, 1949), suggesting that, in basaltic melts, Zn should be predominantly tetrahedrally co-ordinated (Dumas, 1986; Le Grand, 2001). The $K_{D\,Ol/Melt}^{Zn/Mg}$ decreases to lower NBO/T (Non-Bridging Oxygens/Tetrahedrally-Coordinated Cations, Mysen et al., 1988) typical of felsic melt compositions, meaning Zn becomes more incompatible. The coordination of metals in silicate melts decreases with increasing network modifiers (high NBO) with lower bond valence (Farges et al., 2004; Jackson et al., 2005). This provides a basis for the heavy Zn isotope enrichment in liquids, as the lighter isotopes partition into the phase in which Zn has higher coordination (olivine) and therefore weaker Zn-O bonds (cf. Schauble, 2004).

ACCEPTED MANUSCRIPT

These systematics are also affirmed by the Zn isotope composition of spinel, in which tetrahedral Zn is incorporated as the gahnite ($ZnAl_2O_4$) component. At the closure temperature of Zn exchange between spinel and olivine (≈ 850°C), spinel is systematically enriched in $\delta^{66}Zn$ by 0.13‰ relative to the ^{VI}Zn-O bonds of olivine and other Fe-Mg silicates (Wang et al., 2017). Accounting for the effect of temperature on the fractionation factor yields $\Delta^{66}Zn_{Sp\text{-}Ol} = +0.17\times10^6/T^2$ (n = 8). Although Zn partition coefficients between aluminous spinel and melt are roughly 5 times that of olivine (Davis et al., 2013), its modal abundance is too low (<2 ‰) in peridotites to significantly affect the distribution of zinc isotopes, a conclusion also suggested on the grounds that measured whole rocks have similar $\delta^{66}Zn$ to those of Fe-Mg silicates (Wang et al., 2017).

According to the systematics outlined above, the behaviour of Zn and its isotopes can be modelled using the non-modal melting equations developed for element (Shaw, 1970) and isotope (Sossi and O'Neill, 2017) partitioning. Mineral modes, partition coefficients, modal melting reaction coefficients and fractionation factors are shown in Table 2. Both the constancy of Zn content in peridotites over varying degrees of melt extraction (Le Roux et al. 2010; Wang et al., 2017; this work) and the experimentally-measured partition coefficients (Le Roux et al., 2011; Davis et al., 2013) show that $D_{Zn}^{Mantle-Melt} \approx 1$ (here 0.86). Accordingly, partial melts are only mildly enriched in zinc (≈ 65 ppm) with respect to their sources (53.5 ppm) prior to spinel exhaustion, which, if it comprises 2% of the rock, occurs at f = 0.15, using the average of the melting reaction coefficients for low-pressure, clinopyroxene-bearing lherzolites; **(**Wasylenki et al. 2003; Table 2).

$$0.80\,cpx + 0.35opx + 0.10sp = 1liq + 0.25ol \quad (3)$$

In modelling Zn isotope fractionation, the $^{IV}Zn^{2+}$ in spinel is assumed to have the same isotope composition (i.e., force constant) as the $^{IV}Zn^{2+}$ that is presumed to exist in the melt, a feature observed for iron (Dauphas et al., 2014). Insofar as this is correct, an enrichment of +0.08‰ $\delta^{66}Zn$ is modelled in incipient melts relative to the residue (Fig. 3a). This fractionation is only a weak function of f, because the bulk D_{Zn} is close to unity and due to the assumption that spinel and melt have the same zinc isotope composition. This results in primary basaltic liquids with $\delta^{66}Zn$ between +0.22‰ and +0.24‰ for 30% and 0.5% partial melting, or a $\Delta^{66}Zn_{Melt\text{-}Mantle}$ between 0.06‰ and 0.08‰, respectively, at 1573 K. By contrast, because the residual peridotite still contains the bulk of the Zn, mass balance demands that its composition is little affected (up to 0.015‰ lighter at f = 0.3).

ACCEPTED MANUSCRIPT

This has important implications for the Zn isotope heterogeneity in the mantle, because Doucet et al. (2016) suggested that the light isotope composition of refractory peridotites ($\delta^{66}Zn \approx +0.15‰$; [Zn] ≈ 35 ppm) could be caused by 30% melt extraction from fertile peridotites with $\delta^{66}Zn = +0.30‰$, [Zn] ≈ 55 ppm. In a batch melting regime, the fractionation factor and thus the $\delta^{66}Zn$ of the complementary basalts can be calculated from this data alone. In order to produce the observed $\delta^{66}Zn$ and [Zn] drop, $\Delta^{66}Zn_{Melt\text{-}Mantle} = +0.20$ ‰ and $D_{Zn} = 0.36$, with the extracted melt having [Zn] = 102 ppm and $\delta^{66}Zn = +0.42‰$. As illustrated in Fig. 3b, this scenario is incongruous with respect to Zn isotope compositions of terrestrial basalts measured thus far, which vary from +0.2 to +0.3 ‰ in MORB, OIB and continental examples, which, combined with komatiites and peridotites, define a 'mantle array' (this study, Herzog et al. 2009; Chen et al., 2013; Wang et al., 2017). Furthermore, the calculated $\Delta^{66}Zn_{Melt\text{-}Mantle}$ is much larger than that observed for $\Delta^{66}Zn_{Sp\text{-}Ol}$, which, as in the case of $\Delta^{66}Zn_{Melt\text{-}Mantle}$, is presumed to be driven by fractionation between $^{VI}Zn^{2+}$ and $^{IV}Zn^{2+}$. Therefore, $\Delta^{66}Zn_{Melt\text{-}Mantle}$ should be no larger than +0.08‰ (Fig. 3a), hence minimal (<0.015‰ $\delta^{66}Zn$) zinc isotope fractionation occurs in peridotite residues up to 30% partial melting.

5.3.Chemical and isotopic composition of zinc in the Earth's mantle

That measurable zinc isotope fractionation occurs during igneous processes invalidates the assumption that basalts are representative of the BSE, a conclusion already hinted to by isotopically light olivines ($\delta^{66}Zn \approx 0.10‰$) compared to ≈0.25‰ in basaltic rocks (Sossi et al., 2015) and suggested by Wang et al. (2017). Herein, two complementary reservoirs are explored; i) a compilation of peridotitic rocks that sample the lithospheric mantle, and ii) ultramafic magmas (komatiites) that sample the convecting mantle in the Archean. In this way, any sampling bias arising from selecting certain peridotite bodies is alleviated, and the effects of partial melting on the residue and resulting melts can be quantified. Lastly, komatiites also permit a temporal assessment of the evolution of the zinc isotope composition of the Earth's mantle.

In light of Zn isotope fractionation during partial melting, a more accurate representation of the Zn isotope composition of the contemporary mantle is proffered by peridotites compared with basaltic rocks. Although predominantly lherzolitic, sub-ordinate dunites and pyroxenites occur in the Balmuccia massif. Fertile lherzolites representative of the body have Mg# = 0.895, and mildly depleted rare earth element (REE) patterns that are consistent with their origin as residues of 8±2 % melting of primitive mantle (*e.g.* Hartmann and Wedepohl, 1993). Despite

ACCEPTED MANUSCRIPT

a small degree of melt extraction, their Zn contents (48±7 ppm; Table 1) are indistinguishable from the primitive mantle (53.5 ppm; Palme and O'Neill, 2014). Furthermore, the calculations presented above show that 8% partial melting will decrease the δ^{66}Zn of the residue by 0.005 ‰ (i.e., within analytical uncertainty). The insensitivity of the δ^{66}Zn composition of global peridotites to Zn content substantiates the view that even strongly depleted peridotites should preserve unfractionated zinc isotope compositions (Fig. 4). Indeed, the fertile continental lherzolite xenoliths with δ^{66}Zn ≈ +0.30‰ (Doucet et al., 2016) are outliers with respect to all other high-Mg lithologies (including pyroxenites and komatiites; Fig. 4) at similar Zn contents.

A crucial test for the Zn isotope composition of the BSE determined from peridotites, and proof for the rationale outlined above, is provided by mantle-derived magmas formed by high degrees of partial melting, and early in Earth's history to minimise sampling of mantle domains that experienced crust extraction and/or re-fertilisation. Komatiites fulfil both of the above criteria, and can thus be used to constrain the isotopic composition of the early terrestrial mantle, an approach that has been successfully applied to Mg, Fe, Ni, Mo, Ga and Sn isotopes (Dauphas et al., 2010; Nebel et al., 2014; Greber et al., 2015; Gall et al., 2017; Kato et al. 2017; Badullovich et al. 2017). Specifically, komatiites are the result of 25-40% melting of peridotite with a weakly depleted to near-primitive mantle composition at high temperatures (> 1700°C at the locus of melting; Nisbet et al., 1993), both of which act to minimise isotope fractionation (proportional to $1/T^2$). At these conditions, $\Delta^{66}Zn_{Melt\text{-}Mantle} \leq +0.03$‰, meaning that komatiites should faithfully reflect the composition of their sources. As the Archean komatiites analysed herein have sources that were depleted by partial melting degrees between 0 and 5% (Sossi et al., 2016a), they should also be representative of the Archean convecting mantle. Komatiites that separated from both garnet-bearing (Al-depleted) and garnet-absent (Al-undepleted) residues were investigated (Table 1), yet Zn isotopes show no resolvable difference between the two types. Furthermore, there is no apparent correlation with the degree of source depletion; the Munro komatiites, whose sources had already experienced 5% melt extraction (Sossi et al., 2016a), have the same δ^{66}Zn (+0.16‰ and +0.20‰) as the two Cooneterunah komatiites samples, which have flat REE patterns and were derived from primitive mantle. As illustrated in Fig. 3b, given that partial melting engenders heavy Zn isotope enrichment in the complementary melts (section 5.2., see also Doucet et al., 2016), partial melting of a fertile peridotite with δ^{66}Zn ≈ 0.30‰ would not produce primary melts of near-primitive mantle (*i.e.*, komatiites) with δ^{66}Zn ≈ 0.20‰.

ACCEPTED MANUSCRIPT

The origin of the heavier Zn isotopic composition (δ^{66}Zn =+0.30±0.06‰ 2SD) in continental xenoliths is unknown, but the evidence presented hitherto suggest that these samples are unrepresentative of the zinc isotope composition of other peridotites, fertile or otherwise (Wang et al., 2017; Fig. 4), and cannot give rise to the light δ^{66}Zn of mantle-derived magmas (section 5.2.). As a result, they are not considered in the derivation of the δ^{66}Zn value of the primitive mantle. Therefore, combining komatiites with 23 < MgO (wt%) < 33 (i.e., avoiding cumulates) with Balmuccia and remaining literature mantle peridotite data (Doucet et al., 2016; Wang et al., 2017) with MgO >36 wt%, the Earth's upper mantle has δ^{66}Zn = +0.16‰ (*n* = 64, ±0.06‰ 2SD; 0.01‰ 2SE), lighter than previous estimates based on a basalt average (+0.28±0.05‰ 2SD; Chen et al., 2013) and continental xenoliths (+0.30±0.06‰ 2SD; Doucet et al., 2016), but overlapping with the peridotites measured by Wang et al. (2017). The lack of isotope variation between Archean komatiites, aged between 2.7 and 3.5 Ga and sourced from four cratons, and Phanerozoic peridotites further points to the constancy of mantle zinc isotope composition through geologic time and space.

5.4.Chemical and Isotopic Composition of Zinc in the Earth

Before comparisons between the Zn isotope composition between planets and chondrites can be made, the extent of Zn loss to the core must be assessed, and if it occurred, whether isotopic fractionation ensued. Zinc abundances in the BSE are depleted with respect to carbonaceous chondrites, normalised to Mg (Dreibus and Palme 1996; O'Neill and Palme 1998), that is:

$$f_{Zn} = \frac{Zn_x/Mg_x}{Zn_{CI}/Mg_{CI}} \quad (4)$$

Where f_{Zn} refers to the fraction of Zn. For the BSE, f_{Zn} = 0.075 (53.5 ppm, Palme and O'Neill, 2014). Since Zn is not significantly concentrated in the crust, collisional erosion (O'Neill and Palme 2008) is not a strong candidate to account for Zn loss. Three mechanisms may account for such a depletion:

1. Zn was lost to the core
2. Post-accretion volatilisation of Zn
3. Accretion of the planets from material that was initially more volatile-depleted than CI

Given that Zn is overwhelmingly concentrated in silicates and oxides in carbonaceous and ordinary chondrites (Nishimura and Sandell, 1964), it is thought to behave as a lithophile element under the oxygen fugacities typical of these materials. However, under the extremely

ACCEPTED MANUSCRIPT

reducing fO_2s of enstatite chondrites, Zn does partition appreciably into sulfides, along with Ti and the REE (Dreibus and Palme, 1996). Following this logic, the chondritic abundances of Ti and REE in the Earth and on Mars suggest that little Zn was sequestered into the core on either body. Indeed, the greater fraction of FeO in the Martian mantle indicates that core formation took place at higher fO_2 than on Earth (Righter and Drake 1996; Rubie et al. 2004), favouring the retention of Zn in silicates. In S-free systems, the $K_{D_{Zn/Fe}}^{Met/Sil} = 0.1$ (Corgne et al. 2008; Mann et al. 2009), independent of pressure. Although $K_{D_{Zn/Fe}}^{Met/Sil}$ and $D_{Zn}^{Met/Sil}$ climb to maxima of 0.25 and 12, respectively at $X_S^{Met} = 0.5$ (Wood et al. 2014), the Earth's core contains only small quantities of S (1.5 – 2 wt%; Dreibus and Palme, 1996; McDonough, 2003; Suer et al., 2017) and hence will not facilitate Zn incorporation into the Earth's core. Using thermodynamic fits to existing Zn metal-silicate partitioning data, coupled with models of continuous core formation, integrated D_{Zn} between core and mantle varies considerably (between 1 and 6.5), largely as a function of oxygen fugacity. Accordingly, estimates for the Zn content of the bulk Earth span a wide range; 65 to 163 ppm (Mahan et al., 2017). Therefore, given the diversity of accretion models (Rubie et al., 2011), it is possible only to put limits on the amount of Zn in the core.

The relative depletion of Zn in the Earth due to core formation may also be quantified by comparing its abundance to other similarly volatile, but less siderophile elements (Corgne et al. 2007); the alkali metals – Li, Na, K, Rb and Cs plus Mn (Fig. 5). In so doing, ≈30% of the Earth's Zn is expected to reside in the core, corresponding to bulk Zn contents of 81 ppm. Although independent of core formation models, the accuracy of this method is inherently contingent upon the fidelity of condensation temperatures representing elemental volatilities, and is therefore imperfect. Nevertheless, this estimate falls within the range calculated by Mahan et al. (2017). Assuming that no Mg partitioned into the core (Ringwood and Hibberson 1991), the Zn/Mg ratio of the Earth is 3.5×10^{-4}. Importantly, Zn isotopic fractionation attending metal-silicate equilibration is absent to temperatures as low as 1200°C and 1.5 GPa (Bridgestock et al., 2014; Mahan et al., 2017). Therefore, irrespective of the Zn content of the core, the isotope composition of the BSE may be projected to that of the bulk Earth which is therefore $\delta^{66}Zn_{BE} = +0.16\pm0.03$‰.

5.5.Behaviour of zinc during planetary accretion

ACCEPTED MANUSCRIPT

The new estimate of the Earth's $\delta^{66}Zn$ lies on an extension of the carbonaceous chondrite (CC) trend defined by Luck et al. (2005) and Pringle et al. (2017) (Fig. 6), which diagnostic because it extends in a manner perpendicular to fractionation induced by evaporation or condensation, as exemplified by the lunar composition. However, the Earth also overlaps with the zinc isotope composition of high-iron enstatite chondrites (EH; 0.15-0.31‰, Moynier et al., 2011). Such isotopic kinship between EH chondrites and the Earth is also observed for isotopic anomalies for elements such as Cr (Mougel et al. 2017), Ni (Steele et al. 2012), Ti (Zhang et al. 2012) and O (Young et al. 2016) leading to the notion that the Earth is dominantly composed of enstatite chondrites (Javoy et al. 2010) or, at least from similar nebular source material (Wiechert et al., 2001; Dauphas, 2017). However, EHs have Zn/Mg ratios an order of magnitude higher than the Earth (Fig. 6). Subsequent volatile loss by evaporation could then account for the decrease in Zn/Mg_{BE} required, however, this process would be associated with an enrichment in heavy Zn isotopes, a feature not observed (in contrast to the Moon; Kato et al., 2015). Isotopic fractionation may be minimised if it occurred at equilibrium with condensed ZnO in a terrestrial magma ocean or silicates, for which the reaction may be written: (5)

$$ZnO_{(l,s)} = Zn_{(g)} + \frac{1}{2}O_2$$

The temperatures required to decrease the $^{66/64}Zn$ fractionation factor of eq. 5, $\Delta^{66}Zn_{ZnO(s)\text{-}Zn(g)}$, to analytically unresolvable levels (<0.05‰) are >2200°C (given $\Delta^{66}Zn_{ZnO(s)\text{-}Zn(g)} = +0.31\times10^6/2473^2 = +0.05$‰; Ducher et al., 2016). Thermodynamic data for eq. 5 (Lamoreaux et al., 1987) show that the enthalpy and entropy of vaporisation yield Gibbs Free Energies, ΔG^o, of:

$$\Delta G^o{}_{(5)}(kJ/mol) = 411.7 - 0.177T. \quad (6)$$

Vapour pressures of $Zn_{(g)}$ calculated using eq. 6 at 2473 K and 1 bar pressure, given ideality of $ZnO_{(l)}$ in silicate melts (Reyes and Gaskell, 1983) would result in loss of 99.9% of the Zn budget of the residue (see also Canup et al., 2015). Should evaporation of an EH precursor cause the observed depletion of Zn in the BSE (0.075× that of CI or EH), then, at Iron-Wüstite (IW) and 1 bar, temperatures of 1400°C are required, at which $\Delta^{66}Zn_{ZnO(s)\text{-}Zn(g)} = +0.11$‰. The $\delta^{66}Zn$ of the bulk Earth should then reflect the EH average (+0.22±0.06‰) plus $\Delta^{66}Zn_{ZnO(s)\text{-}Zn(g)}$, equal to +0.33‰, heavier than that observed. The isotopic composition of another lithophile MVE, Rb, in the Earth (Pringle and Moynier, 2017) also falls on the end of a carbonaceous chondrite array in a plot of $^{87}Rb/^{85}Rb$ *vs.* Rb/Sr (Sr is used as the normalising refractory lithophile element

ACCEPTED MANUSCRIPT

analogous to Mg herein). Due to the different equilibrium partial pressures and evaporation stoichiometries of of $Rb_{(g)}$ and $Zn_{(g)}$, the fact that both isotopic systems constrain the Earth to lie at the volatile-depleted end of the CC array strongly argues against vaporisation of a volatile-rich, isotopically light precursor.

Rather, the recognition that Earth falls at the volatile-depleted end of the CC array for both Rb and Zn isotopes allows a simpler interpretation; that the Earth accreted from material that experienced chemical and isotopic fractionation in the solar nebula in the same manner as the CCs, but proceeded to more volatile-depleted extremes. Although carbonaceous chondrites, given their disparate O and other mass-independent isotope signatures compared to the Earth (*e.g.*, Clayton et al., 1976; Budde et al., 2016), are not considered its primary constituents, similarities in elemental abundances between Earth and CCs suggest they underwent similar chemical evolution in the solar nebula. Specifically, the Earth shares comparable refractory lithophile element ratios (Palme and O'Neill, 2014) with carbonaceous chondrites and has volatile/refractory element ratios (*e.g.,* K/U vs Rb/Sr, and Mn/Na) that plot along an array defined by CCs, except to more volatile-depleted values, as per Fig. 6 (Halliday and Porcelli, 2001; O'Neill and Palme, 2008; Wang et al. 2016). Together, these factors imply that the Earth had its Zn complement set by processes operative during the formation of carbonaceous chondrites.

The nebular origin of zinc in the Earth precludes any significant loss of Zn during a potential Moon-forming giant impact, despite evidence for vaporisation from the Moon (Paniello et al., 2012). The volatile budget of the Moon is markedly depleted with respect to the BSE (O'Neill, 1991; Taylor and Wieczorek, 2014). Planetary-scale impacts between differentiated planetesimals typify the later stages of accretion (*e.g.,* Morbidelli et al., 2012), which, in the case of the giant impact, occur some 70-110 Myr after chondrite formation (Halliday, 2008). Here, volatile loss would occur at oxygen fugacities defined by the evaporation of planetary mantles, whose dominant gas species, $SiO_{(g)}$, buffers fO_2 near fayalite-magnetite-quartz (FMQ), $\approx 10^7$ times more oxidising than the nebular gas (Visscher and Fegley, 2013). This consideration is important because element volatility depends on the redox state of the gas:

$$\left(M^x \frac{x}{2} O\right) + \frac{n}{4} O_2 = \left(M^{x+n} \frac{x+n}{2} O\right),$$

ACCEPTED MANUSCRIPT

where, even at FMQ, the stable gas species for many MVEs, including Zn, is the monatomic gas (Lamoreaux et al., 1987). However, MVE speciation in the condensed phases differs, such that the relative volatilities of element pairs changes with fO_2. One notable example is Mn/Na; $Mn^{2+}O$ and $Na^{+}O_{0.5}$ are stable in liquids or solids, whereas $Mn_{(g)}$ and $Na_{(g)}$ are the equilibrium gas species. Therefore, the ratio of their vapour pressures, pNa/pMn is proportional to $fO_2^{1/4}$ (eq. 7), such that Na becomes relatively more volatile than Mn at high fO_2 (O'Neill and Palme, 2008). This ratio is used to discern between nebular (reducing) and post-nebular (oxidising) volatile depletion, where basalts from small telluric bodies in the inner solar system, including the Moon, exhibit elevated Mn/Na with respect to chondrites. The extent of orthogonal deviation of the Moon from the chondritic array Zn/Mg-δ^{66}Zn is correlative with its Mn/Na ratio (Fig. 7), fingerprinting post-nebular fractionation. By contrast, carbonaceous chondrites show little variation in Mn/Na (indicating similar T_C), whereas the Earth falls at the end of the CC trend. Thus, the Earth's chondritic Mn/Na ratio is further evidence that it was set by nebular processes. The fact that Zn, whose vaporisation stoichiometry mirrors that of Mn, preserves a nebular isotope signature implies that MVEs with similar volatility to Zn (*e.g.* K), or with the same volatility dependence with fO_2 (*e.g.* Fe^{2+}), were not lost from the Earth in an impact scenario. This is consistent with numerical models of protolunar disk evolution, in which most of the disk's volatile components may be transported to Earth rather than being lost to space (Charnoz and Michaut, 2015). Furthermore, this implies that MVE isotope systems should be unfractionated in the BSE with respect to the systematics found in chondrites, as observed for K, Li, Cd, Ga, Cl and Rb isotopes (Wang and Jacobsen 2016; Magna et al., 2006; Sharp et al., 2007; Wombacher et al., 2008; Nebel et al., 2011; Pringle and Moynier 2017; Kato et al., 2017).

The observation that the depletion factors of moderately volatile elements in the Earth resemble those in silicate liquid residues of evaporation at 1300°C near the IW buffer led Norris and Wood (2017) to conclude that Earth's MVE budget, including siderophile (*e.g.* Ag, Ge) and lithophile (*e.g.* Zn, Tl) elements, were set solely by evaporative loss from silicate melts during accretion. For this interpretation to hold, it implies that either i) core formation had limited impact on the budgets of MVEs in the Earth or ii) the MVEs were accreted from residues of material that had experienced evaporative loss, after the cessation of core formation. The first scenario is unappealing due to the well-documented depletion of other non-volatile siderophile elements (*e.g.* Ni, Co, W) due to core formation (*e.g.*, Schmitt et al., 1989). The second should be accompanied by resolvable mass-dependent fractionation in the stable isotopes of moderately volatile elements (*e.g.*, Wombacher et al., 2004; Yu et al., 2003), which is not

ACCEPTED MANUSCRIPT

observed, as stated above. Although fractionation is recorded for Mg isotopes and taken as evidence for vaporisation (Hin et al., 2017), heavy isotope enrichments also characterise the two other main components, Fe (Sossi et al., 2016b) and Si (Armytage et al., 2011), a characteristic attributed to nebular volatile depletion on Earth (Sossi et al., 2016b). Therefore, there is currently no consensus as to the locus or timing of volatile depletion that afflicted the Earth. Given the evidence presented, we propose that the MVE depletion in the Earth is of nebular origin, and henceforth investigate the delivery of moderately volatile elements in the framework of their accretion to the Earth from chondritic components.

5.6.Implications for Accretion of Other Moderately Volatile Elements to the Earth

In the short-lived ^{53}Mn-^{53}Cr ($T_{1/2}$=3.7 Myrs) system, where Mn is more volatile than Cr, the BSE falls on an external isochron defined by carbonaceous chondrites, also signifying that Earth's Mn budget was set at the commencement of the solar system (Moynier et al., 2007). By contrast, Pb and Ag-Pd isotope systematics require late volatile addition (Schönbächler et al., 2010; Albarède et al., 2013); either a small (≈2-5%) CI chondrite component, or a larger (≈10–15%) fraction of a CO/CV-like composition (Albarède et al., 2013).

To simulate the chemical effects of late volatile delivery, a model is constructed in which different fractions of CI- or CV chondrites (≤5% and ≤15%. respectively; Albarède et al., 2013) are added to a proto-Earth's mantle whose abundances of Mn, Rb, In, Zn, Ag and Pb are found by least-squares minimisation where their final concentrations (proto-Earth + CI/CV) must match the contemporary BSE (Palme and O'Neill, 2014). In the limiting case of addition of 5% CI or 15% CV chondrites, they contribute about 15 ppm (300×0.05 or 100×0.15) of the contemporary 53.5 ppm of Zn observed, meaning ≥75% of the Earth's present-day Zn would already be present in the proto-Earth (Fig. 8). As Zn is correlated with other MVEs in chondrites (Wasson and Kallemeyn, 1988) as well as water (Albarède et al.. 2013), other weakly siderophile or lithophile MVEs, In, Mn and Rb are also remnants of early accretion (Fig. 8), as further suggested by the isotopic composition of Rb in the Earth (Pringle and Moynier, 2017). Therefore, should the early accretion of the Earth be typified by reduced material, then this must also contain the majority of its lithophile MVE budget. Contrastingly, late volatile addition contributes to most of Pb and particularly Ag observed in the primitive mantle (Fig. 8). For Pb, for example, CIs contain 2.4 ppm, therefore a 5% addition would deliver 0.12 ppm, or 65%, of the 0.185 ppm present today.

ACCEPTED MANUSCRIPT

The early accretion of Rb (Halliday and Porcelli, 2001), Mn (O'Neill and Palme, 2008) and Zn contrasted with the late delivery of Ag and Pb (Schönbächler et al., 2010; Albarède et al., 2013) can be reconciled with the early partitioning of the latter into the core. Lead and Ag are particularly chalcophile, and become siderophile under the very reducing conditions prevailing during early core formation on the Earth (Mann et al., 2009; Wood et al., 2008). Therefore, even if Ag-Pb were added in the early stages of accretion, their concentrations would have been reduced to almost nil in the silicate portion of the proto-Earth following core formation. By contrast, Zn, Mn and particularly Rb would have remained in high abundances due to their lithophile character. In this case, the fraction that late accreting material would contribute to an element's present-day BSE abundance decreases in the order Rb ≈ Mn < Zn ≤ In < Pb < Ag (Fig. 8), broadly roportional to their metal-silicate partition coefficients. Therefore, the robust conclusion can be drawn that the bulk of the Zn (and other moderately volatile lithophile elements) and hence their isotopic composition were inherited from the Earth's precursor material, which is itself more volatile depleted than, though on the same trend as, the carbonaceous chondrites.

Conclusions

A complementary dataset comprising ultramafic rocks, both peridotites and komatiites, is used to quantify processes that cause Zn isotope variations in the terrestrial mantle. A general trend of falling δ^{66}Zn with increasing MgO is observed. Together with published data on peridotitic rocks and their constituent minerals, it is demonstrated that partial melting is ineffective in producing Zn isotope fractionation in the mantle. However, the complementary partial melts may be significantly enriched in the heavier isotopes of Zn, such that they are up to +0.08‰ heavier than their sources. The high temperatures and degrees of melting that produce komatiites mitigate this effect such that they reflect the Zn isotope composition of their sources, with no variation according to age, source depletion or petrogenetic type. Thus, a compilation of 60 ultramafic rocks defines the composition of the Bulk Silicate Earth to +0.16±0.06‰. After accounting for partial Zn removal in the terrestrial core (which engenders no isotopic fractionation), the bulk Earth falls to the volatile depleted end of the carbonaceous chondrite array in a δ^{66}Zn vs log(Zn/Mg) plot. The preservation of these systematics suggests that Zn (and elements less volatile) in the Earth records its initial nebular composition, and was not modified thereafter during a putative Moon-forming collision. By contrast, the Moon falls off

ACCEPTED MANUSCRIPT

the chondritic array to higher δ^{66}Zn and lower log (Zn/Mg), to an extent correlative with its Mn/Na, a fingerprint of oxidising, post-nebular volatile loss on this body.

References

Albarède F., Ballhaus C., Blichert-Toft J., Lee C. T., Marty B., Moynier F. and Yin Q. Z. (2013) Asteroidal impacts and the origin of terrestrial and lunar volatiles. *Icarus* 222, 44–52.

Allen R. O. and Mason B. (1973) Minor and trace elements in some meteoritic minerals. *Geochim. Cosmochim. Acta* 37, 1435–1456.

Armytage R.M.G., Georg R.B., Savage P.S., Williams H.M. and Halliday A.N. (2011). Silicon isotopes in meteorites and planetary core formation. *Geochim. Cosmochim. Acta* 75, 3662–3676.

Badullovich N., Moynier F., Creech J., Teng F. and Sossi P. A. (2017) Tin isotopic fractionation during igneous differentiation and Earth's mantle composition. *Geochemical Perspect. Lett.* 5, 24–28.

Ballhaus C., Laurenz V., Münker C., Fonseca R. O. C., Albarède F., Rohrbach A., Lagos M., Schmidt M. W., Jochum K.-P., Stoll B., Weis U. and Helmy H. M. (2013). The U/Pb ratio of the Earth's mantle—A signature of late volatile addition. *Earth Planet. Sci. Lett.* 362, 237–245.

Bridgestock L. J., Williams H., Rehkämper M., Larner F., Giscard M. D., Hammond S., Coles B., Andreasen R., Wood B. J., Theis K. J., Smith C. L., Benedix G. K. and Schönbächler M. (2014) Unlocking the zinc isotope systematics of iron meteorites. *Earth Planet. Sci. Lett.* 400, 153–164.

Budde G., Burkhardt C., Brennecka G. A., Fischer-Gödde M., Kruijer T. S., & Kleine T. (2016). Molybdenum isotopic evidence for the origin of chondrules and a distinct genetic heritage of carbonaceous and non-carbonaceous meteorites. *Earth Planet. Sci. Lett.*, 454, 293-303.

Canup R. M., Visscher C., Salmon J., Fegley Jr B. (2015). Lunar Volatile Depletion Due To Incomplete Accretion Within An Impact-Generated Disk. *Nat. Geosci*. 8, 1–6.

Charnoz S. and Michaut C. (2015). Evolution of the protolunar disk: Dynamics, cooling timescale and implantation of volatiles onto the Earth. *Icarus* 260, 440–463.

Chen H., Savage P. S., Teng F.-Z., Helz R. T. and Moynier F. (2013). Zinc isotope fractionation during magmatic differentiation and the isotopic composition of the bulk Earth. *Earth Planet. Sci. Lett.* 369-370, 34–42.

Clayton R. N., Onuma,N. and Mayeda T. K. (1976). A classification of meteorites based on oxygen isotopes. *Earth Planet. Sci. Lett.* 30(1), 10-18.

Corgne A., Keshav S., Fei Y. and McDonough W. F. (2007) How much potassium is in the Earth's core? New insights from partitioning experiments. *Earth Planet. Sci. Lett.* 256, 567–576.

Corgne A., Keshav S., Wood B.J. McDonough W. F. and Fei, Y. (2008) Metal–silicate partitioning and constraints on core composition and oxygen fugacity during Earth accretion. *Geochim. Cosmochim. Acta* 72, 574–589.

Davis F. A., Humayun M., Hirschmann M. M. and Cooper R. S. (2013) Experimentally determined mineral/melt partitioning of first-row transition elements (FRTE) during partial melting of peridotite at 3GPa. *Geochim. Cosmochim. Acta* 104, 232–260.

Dauphas N., Roskosz M., Alp E.E., Neuville D.R., Hu M.Y., Sio C.K., Tissot F.L.H., Zhao J., Tissandier L., Médard E. and Cordier C. (2014). Magma redox and structural controls on iron isotope variations in Earth's mantle and crust. *Earth Planet. Sci. Lett.* 398, 127–140.

ACCEPTED MANUSCRIPT

Dauphas, N., Teng, F.-Z., Arndt, N.T. (2010). Magnesium and iron isotopes in 2.7 Ga Alexo komatiites: Mantle signatures, no evidence for Soret diffusion, and identification of diffusive transport in zoned olivine. *Geochim. Cosmochim. Acta* 74, 3274–3291.

Dauphas N. (2017). The isotopic nature of the Earth's accreting material through time. *Nature*, 541, 521-524.

Day J. M. D. and Moynier F. (2014) Evaporative fractionation of volatile stable isotopes and their bearing on the origin of the Moon. *Philos. Trans. R. Soc. A* 372, 1–26.

Donaldson C. H. (1976). An experimental investigation of olivine morphology. *Contrib. Mineral. Petrol.* 57(2), 187-213.

Doucet L. S., Mattielli N., Ionov D. A., Debouge W. and Golovin A. V. (2016). Zn isotopic heterogeneity in the mantle: A melting control? *Earth Planet. Sci. Lett.*, 451, 232-240.

Dreibus G. and Palme H. (1996) Cosmochemical constraints content in the Earth's core. *Geochim. Cosmochim. Acta* 60, 1125–1130.

Ducher M., Blanchard M., Balan E. (2016) Equilibrium zinc isotope fractionation in Zn-bearing minerals from first-principles calculations. Chem. Geol. 443, 87–96.

Dumas T. and Petiau J. (1986) EXAFS study of titanium and zinc environments during nucleation in a cordierite glass. *J. Non. Cryst. Solids* 81, 201–220.

Ebel, D. S., Brunner, C., Konrad, K., Leftwich, K., Erb, I., Lu, M., Rodriguez, H., Crapster-Pregont, E. J., Friedrich, J. M. & Weisberg, M. K. (2016). Abundance, major element composition and size of components and matrix in CV, CO and Acfer 094 chondrites. Geochimica et Cosmochimica Acta, 172, 322-356.

Farges F., Lefrère Y., Rossano S., Berthereau A., Calas G. and Brown G. E. (2004). The effect of redox state on the local structural environment of iron in silicate glasses: a combined XAFS spectroscopy, molecular dynamics, and bond valence study. *J. Non-Crys. Solids* 344(3), 176-188.

Gall L., Williams H. M., Halliday A. N. and Kerr A. C. (2017). Nickel isotopic composition of the mantle. *Geochim. Cosmochim. Acta*, 199, 196-209.

Greber N. D., Puchtel I. S., Nägler T. F. and Mezger K. (2015). Komatiites constrain molybdenum isotope composition of the Earth's mantle. *Earth Planet. Sci. Lett.*, 421, 129-138.

Halliday A. N. and Porcelli D. (2001). In search of lost planets - the paleocosmochemistry of the inner solar system. *Earth Planet. Sci. Lett.* 192, 545–559.

Halliday A. N. (2008). A young Moon-forming giant impact at 70–110 million years accompanied by late-stage mixing, core formation and degassing of the Earth. *Phil. Trans. R. Soc. A.* 366, 4163-4181.

Hartmann G. and Wedepohl K. H. (1993). The composition of peridotite tectonites from the Ivrea Complex, northern Italy: Residues from melt extraction. *Geochim. Cosmochim. Acta* 57, 1761–1782.

Herzog G.F., Moynier F., Albarède F., Berezhnoy A.A. (2009) Isotopic and elemental abundances of copper and zinc in lunar samples, Zagami, Pele's hairs, and a terrestrial basalt. *Geochim. Cosmochim. Acta* 73, 5884–5904.

Humayun M. and Clayton R. N. (1995). Potassium isotope cosmochemistry: Genetic implications of volatile element depletion. *Geochim. Cosmochim. Acta* 59, 2131–2148.

Humayun M. and Cassen P. (2000). Processes Determining the Volatile Abundances of the Meteorites and Terrestrial Planets. *In:* Canup R.M., Righter K. (eds.) *The Origin of the Earth and Moon*. University of Arizona Press, Tucson, pp 3–23

Jackson, W. E., Farges, F., Yeager, M., Mabrouk, P. A., Rossano, S., Waychunas, G. A., Solomon, E. I. and Brown, G. E. (2005). Multi-spectroscopic study of Fe (II) in silicate glasses: Implications for the coordination environment of Fe (II) in silicate melts. *Geochim. Cosmochim. Acta*, 69(17), 4315-4332.

ACCEPTED MANUSCRIPT

Javoy M., Kaminski E., Guyot F., Andrault D., Sanloup C., Moreira M., Jambon A., Arginier A., Davaille A. & Jaupart C. (2010). The chemical composition of the Earth: Enstatite chondrite models. *Earth Planet. Sci. Lett.*, 293(3), 259-268.

Kato C., Moynier F., Valdes M. C., Dhaliwal J. K., and Day J. M. (2015). Extensive volatile loss during formation and differentiation of the Moon. *Nature Comm.*, 6, 7617.

Kato C., Moynier F., Foriel, J., Teng F. Z., & Puchtel I. S. (2017). The gallium isotopic composition of the bulk silicate Earth. *Chem. Geol.*, 448, 164-172.

Kinzler R. J., and Grove T. L. (1985). Crystallization and differentiation of Archean komatiite lavas from Northeast Ontario; phase equilibrium and kinetic studies. *Am. Min.* 70(1-2), 40-51.

Kohn S. C. and Schofield P. F. (1994) The importance of melt composition in controlling trace-element behaviour: an experimental study of Mn and Zn partitioning between forsterite and silicate melts. *Chem. Geol.* 117, 73–87.

Lamoreaux R. H., Hildenbrand D. L. and Brewer, L. (1987). High-Temperature Vaporization Behavior of Oxides II. Oxides of Be, Mg, Ca, Sr, Ba, B, Al, Ga, In, Tl, Si, Ge, Sn, Pb, Zn, Cd, and Hg. *J. Phys. Chem. Ref. Data* 16, 419-443.

Le Grand M., Ramos A. Y., Calas G., Galoisy L., Ghaleb D. and Pacaud F. (2000) Zinc environment in aluminoborosilicate glasses by Zn K-edge extended X-ray absorption fine structure spectroscopy. *J. Mater. Res.* 15, 2015–2019.

Le Roux, V., Dasgupta, R. and Lee, C. T. A. (2011). Mineralogical heterogeneities in the Earth's mantle: Constraints from Mn, Co, Ni and Zn partitioning during partial melting. *Earth Planet. Sci. Lett.* 307(3), 395-408.

Le Roux, V., Lee, C. T. A. and Turner, S. J. (2010). Zn/Fe systematics in mafic and ultramafic systems: Implications for detecting major element heterogeneities in the Earth's mantle. *Geochim. Cosmochim. Acta*, 74(9), 2779-2796.

Lodders K. (2003) Solar System Abundances and Condensation Temperatures of the Elements. *Astrophys. J.* 591, 1220–1247.

Luck J.-M., Ben Othman D. and Albarède F. (2005) Zn and Cu isotopic variations in chondrites and iron meteorites: Early solar nebula reservoirs and parent-body processes. *Geochim. Cosmochim. Acta* 69, 5351–5363.

Magna T., Wiechert U. and Halliday A. N. (2006) New constraints on the lithium isotope compositions of the Moon and terrestrial planets. *Earth Planet. Sci. Lett.* 243, 336–353.

Mann U., Frost D. J. and Rubie D. C. (2009) Evidence for high-pressure core-mantle differentiation from the metal–silicate partitioning of lithophile and weakly-siderophile elements. *Geochim. Cosmochim. Acta* 73, 7360–7386.

McDonough W. F. (2003) Compositional model for the Earth's core. In: Carlson, R. W. (ed) *Treatise on Geochemistry, vol. 2*. Elsevier, Amsterdam, pp 547–568

Mahan B., Siebert J., Pringle E. A. and Moynier F. (2017). Elemental partitioning and isotopic fractionation of Zn between metal and silicate and geochemical estimation of the S content of the Earth's core. *Geochim. Cosmochim. Acta* 196, 252-270.

Makishima A., Nakamura E. (2013). Low-blank chemistry for Zn stable isotope ratio determination using extraction chromatographic resin and double spike-multiple collector-ICP-MS. *J. Anal. At. Spectrom.*, 28, 127–133.

Mazzucchelli M., Rivalenti G., Brunelli D., Zanetti A. and Boari E. (2008). Formation of highly refractory dunite by focused percolation of pyroxenite-derived melt in the Balmuccia peridotite massif (Italy). *J. Petrol.* 50(7), 1205-1233.

ACCEPTED MANUSCRIPT

Morbidelli A., Lunine J. I., O'Brien D. P., Raymond S. N. and Walsh K. J. (2012) Building Terrestrial Planets. *Annu. Rev. Earth Planet. Sci.* 40, 251–275.

Moynier F., Paniello R. C., Gounelle M., Albarède F., Beck P., Podosek F. A. and Zanda B. (2011) Nature of volatile depletion and genetic relationships in enstatite chondrites and aubrites inferred from Zn isotopes. *Geochim. Cosmochim. Acta* 75, 297–307.

Moynier F., Yin Q. and Jacobsen B. (2007) Dating the First Stage of Planet Formation. *Astrophys. J.* 671, 181–183.

Nebel O., Campbell I.H., Sossi P.A., Van Kranendonk M.J. (2014). Hafnium and iron isotopes in early Archean komatiites record a plume-driven convection cycle in the Hadean Earth. *Earth Planet. Sci. Lett.* 397, 111–120.

Nebel O. Mezger K. and van Westrenen W. (2011) Rubidium isotopes in primitive chondrites: Constraints on Earth's volatile element depletion and lead isotope evolution. *Earth Planet. Sci. Lett.* 305, 309–316.

Neumann H. (1949) Notes on the mineralogy and geochemistry of zinc. *Mineral. Mag.* 28, 575–581.

Nisbet E. G., Cheadle M. J., Arndt, N. T. and Bickle, M. J. (1993). Constraining the potential temperature of the Archaean mantle: a review of the evidence from komatiites. *Lithos* 30(3-4), 291-307.

Nishimura M. and Sandell E. B. (1964) Zinc in meteorites. *Geochim. Cosmochim. Acta* 28, 1055–1079.

Obermiller, W., 1994. Chemical and isotopic variations in the Balmuccia, Baldissero and Finero peridotite massifs (Ivrea Zone, N-Italy). *PhD Thesis.* Max Planck Institut, Mainz.

O'Neill, H. S. C. (1991). The origin of the Moon and the early history of the Earth—A chemical model. Part 1: The Moon. *Geochim. Cosmochim. Acta*, 55(4), 1135-1157.

O'Neill, H. S. C. and Palme, H. (1998). Composition of the Silicate Earth: Implications for Accretion and Core Formation. In: Jackson I (ed) *The Earth's Mantle: Composition, Structure and Evolution*. Cambridge University Press, Cambridge, pp 3 – 126

O'Neill H. S. C. and Palme H. (2008) Collisional erosion and the non-chondritic composition of the terrestrial planets. *Philos. Trans. A. Math. Phys. Eng. Sci.* 366, 4205–38.

Palme H. and O'Neill H. S. C. (2014). Cosmochemical estimates of mantle composition. *In*: (Carlson R., *ed.*,) Treatise of Geochemistry 2nd Edition, vol. 3: The Mantle and Core. 1-39.

Paniello R. C., Day J. M. D. and Moynier F. (2012) Zinc isotopic evidence for the origin of the Moon. *Nature* 490, 376–9.

Pringle E. A., Moynier F., Beck P., Paniello R. and Hezel D. C. (2017). The origin of volatile element depletion in early solar system material: Clues from Zn isotopes in chondrules. *Earth Planet. Sci. Lett.*, 468, 62-71.

Pringle E. A. & Moynier F. (2017). Rubidium isotopic composition of the Earth, meteorites, and the Moon: Evidence for the origin of volatile loss during planetary accretion. *Earth Planet. Sci. Lett.*, 473, 62-70.

Reyes R. A. & Gaskell D. R. (1983). The thermodynamic activity of ZnO in silicate melts. *Metallurgical Transactions B*, 14(4), 725-731.

Richter F.M., Davis A.M., Ebel D.S., Hashimoto A. (2002). Elemental and isotopic fractionation of type B calcium-, aluminum-rich inclusions: Experiments, theoretical considerations, and constraints on their thermal evolution. *Geochim. Cosmochim. Acta* 66, 521–540.

Righter, K., Drake, M. J. (1996). Core Formation in Earth's Moon, Mars, and Vesta. *Icarus*, 124, 513–529.

Ringwood A. E. and Hibberson W. (1991). Solubilities of mantle oxides in molten iron at high pressures and temperatures: implications for the composition and formation of Earth's core. *Earth Planet Sci Lett* 102, 235–251.

Rivalenti G., Mazzucchelli M. Vannucci R., Hofmann A. W., Ottolini L., Bottazzi P. and Obermiller W. (1995).

ACCEPTED MANUSCRIPT

The relationship between websterite and peridotite in the Balmuccia peridotite massif (NW Italy) as revealed by trace element variations in clinopyroxene. *Contrib. Mineral. Petrol.* 121(3), 275-288.

Rubie D. C., Gessmann C. K. and Frost D. J. (2004). Partitioning of oxygen during core formation on the Earth and Mars. *Nature* 429, 58–61.

Rubie D. C., Frost D. J., Mann U., Asahara Y., Nimmo F., Tsuno K., Kegler P., Holzheid A. and Palme H. (2011). Heterogeneous accretion, composition and core–mantle differentiation of the Earth. *Earth Planet. Sci. Lett.* 301(1), 31-42.

Schauble, E. A. (2004). Applying stable isotope fractionation theory to new systems. *Rev. Mineral. Geochem.*, 55(1), 65-111.

Schmitt W., Palme H., Wänke H. (1989). Experimental determination of metal / silicate partition coefficients for P, Co, Ni, Cu, Ga, Ge, Mo, and W and some implications for the early evolution of the Earth. *Geochim. Cosmochim. Acta* 53, 173–185.

Schönbächler M., Carlson R. W., Horan M. F., Mock T. D. and Hauri E. H. (2010). Heterogeneous accretion and the moderately volatile element budget of Earth. *Science* 328, 884–7.

Sharp Z. D., Barnes J. D., Brearley A. J., Chaussidon M., Fischer T. P. and Kamenetsky V. S. (2007) Chlorine isotope homogeneity of the mantle, crust and carbonaceous chondrites. *Nature* 446, 1062–5.

Shervais, J. W. and Mukasa, S. B. (1991). The Balmuccia orogenic lherzolite massif, Italy. *J. Petrol.* 2, 155-174.

Sivry, Y., Riotte, J., Sonke, J. E., Audry, S., Schäfer, J., Viers, J., Blanc, G., Freydier, R. and Dupré, B. (2008). Zn isotopes as tracers of anthropogenic pollution from Zn-ore smelters The Riou Mort–Lot River system. *Chem. Geol.* 255(3), 295-304.

Sossi P. A., Halverson G. P., Nebel O. and Eggins S. M. (2015). Combined separation of Cu, Fe and Zn from rock matrices and improved analytical protocols for stable isotope determination. *Geostand. Geoanalytical Res.* 39, 129–149.

Sossi P. A., Nebel O., Anand M. and Poitrasson F. (2016a). On the iron isotope composition of Mars and volatile depletion in the terrestrial planets. *Earth Planet. Sci. Lett.* 449, 360-371.

Sossi P. A., Eggins S. M., Nesbitt R. W., Nebel O., Hergt J. M., Campbell I. H., O'Neill H. S. C., Van Kranendonk M. and Davies D. R. (2016b). Petrogenesis and Geochemistry of Archean Komatiites. *J. Petrol.* 57, 147–184.

Sossi P. A. and O'Neill H. S. C. (2017). The effect of bonding environment on iron isotope fractionation between minerals at high temperature. *Geochim. Cosmochim. Acta* 196, 121-143.

Suer T. A., Siebert J., Remusat L., Menguy N. & Fiquet, G. (2017). A sulfur-poor terrestrial core inferred from metal–silicate partitioning experiments. *Earth Planet. Sci. Lett.*, 469, 84-97.

Sulcek Z. and Povondra P. (1989). Methods of decomposition in inorganic analysis. *CRC press*. pp. 325.

Taylor G. J. and Wieczorek M. A. (2014). Lunar bulk chemical composition: a post-Gravity Recovery and Interior Laboratory reassessment. *Phil. Trans. R. Soc. A*, 372(2024), 20130242.

Toplis, M. J. (2005). The thermodynamics of iron and magnesium partitioning between olivine and liquid: criteria for assessing and predicting equilibrium in natural and experimental systems. *Contrib. Mineral. Petrol.*, 149(1), 22-39.

Visscher C. and Fegley B. (2013). Chemistry of impact-generated silicate melt-vapor debris disks. *Astrophys. J. Lett.* 767(L12).

Wang K., Jacobsen S. B. (2016). Potassium Isotopic Evidence for the Origin of the Moon. *Nature* 538, 487–490.

Wang Z., Laurenz V., Petitgirard S. and Becker H. (2016). Earth's moderately volatile element composition may not be chondritic: Evidence from In, Cd and Zn. *Earth Planet. Sci. Lett.* 435, 136–146.

ACCEPTED MANUSCRIPT

Wang Z.-Z., Liu S.-A., Liu, J., Huang J., Xiao Y., Chu Z.-Y., Zhao X.-M. and Tang L. (2017). Zinc isotope fractionation during mantle melting and constraints on the Zn isotope composition of Earth's upper mantle. *Geochim. Cosmochim. Acta*, 198, 151-167.

Wasson J. T. and Kallemeyn G. W. (1988). Compositions of Chondrites. *Philos. Trans. R. Soc. A* 325, 535–544.

Wasylenki L. E., Baker M.B., Kent A.J.R., Stolper E.M. (2003). Near-solidus Melting of the Shallow Upper Mantle : Partial Melting Experiments on Depleted Peridotite. *Contrib. Mineral. Petrol.* 44 (1163–1191).

Wiechert U., Halliday A. N., Lee D. C., Snyder G. A., Taylor L. A. , Rumble D. (2001). Oxygen isotopes and the moon-forming giant impact. *Science* 294, 345-348

Wilke M. (2005). Fe in magma – An overview. *Ann. Geophys.* 48, 609–617.

Wombacher, F., Rehkämper, M., & Mezger, K. (2004). Determination of the mass-dependence of cadmium isotope fractionation during evaporation. *Geochim. Cosmochim. Acta*, 68(10), 2349-2357.

Wombacher F., Rehkämper M., Mezger K., Bischoff A. and Münker C. (2008). Cadmium stable isotope cosmochemistry. *Geochim. Cosmochim. Acta* 72, 646–667.

Wood B. J. and Halliday A. N. (2010). The lead isotopic age of the Earth can be explained by core formation alone. *Nature* 465, 767–70.

Wood B. J., Kiseeva E. S. and Mirolo F. J. (2014) Accretion and core formation: the effects of sulfur on metal-silicate partition coefficients. *Geochim. Cosmochim. Acta*, 148, 248-267

Yu Y., Hewins R. H., Alexander C. M. O 'D., Wang J. (2003). Experimental study of evaporation and isotopic mass fractionation of potassium in silicate melts. *Geochim. Cosmochim. Acta*, 67, 773–786.

ACCEPTED MANUSCRIPT

ACCEPTED MANUSCRIPT

Figure Captions

Fig. 1. *[2 columns]* The change in zinc isotope composition for the samples studied in this work, expressed as δ^{66}Zn, as a function of **a)** MgO (wt. %) and **b)** Zn (ppm) content of the whole rocks. Uncertainties are 2SD.

Fig. 2. *[1 column]* The Zn/Fe ratios in Spinifex-Textured Komatiites and Spinifex-Textured Basalts as a function of their MgO contents. Balmuccia peridotites and the primitive mantle (red star) are also shown. In black, the fractional crystallisation/accumulation of olivine is shown, with black circles representing 10% increments of olivine addition/subtraction. Symbols as per Fig. 1.

Fig. 3. *[2 columns]* A compilation of the zinc isotope compositions of mantle melts with two melting models overlain **a)** partition coefficients and fractionation factors deduced from parameters listed in Table 2 and **b)** partition coefficients and fractionation factors inferred from Doucet et al. (2016) assuming refractory peridotites (purple circles) are residues after 30% melt extraction from a primitive mantle source (yellow circles), as modelled by the black line. In this case modelled partial melts (red line) are much heavier than observed (red squares, OIBs (Kilauea) - Chen et al. 2013; blue squares, MORBs – Wang et al., 2017; green squares, STK and green diamonds, Balmuccia peridotites – this work). These define a 'mantle array' which passes through the Balmuccia peridotites and the refractory peridotites of Doucet et al. (2016).

Fig. 4. *[1 column]* Determination of the zinc isotope composition of the BSE. Circles in green denote all peridotite samples in the literature (Doucet et al., 2016; Wang et al., 2017; this study) save for the fertile continental xenoliths shown in yellow (Doucet et al., 2016). Dark green squares are spinifex-textured komatiites (this study).

Fig. 5. *[1 columns]* Relative abundances of moderately-volatile elements, expressed as depletion factors, in the Earth (Palme and O'Neill, 2014; green squares) and carbonaceous chondrites (diamonds; Wasson and Kallemeyn, 1988), normalised to Mg and CI-chondrites. They are plotted in accord with their half-condensation temperatures, T_C (K) from Lodders (2003). The terrestrial trend is estimated from the depletion factors of alkali metals and Mn.

Fig. 6. *[2 columns]* Zinc isotope compositions of planetary materials. Carbonaceous chondrites (Luck et al., 2005; Pringle et al., 2017) are plotted as diamonds, ordinary chondrites (Luck et al., 2005) as circles and enstatite chondrites (Moynier et al., 2011) as squares. The bulk Earth (green) plots on the carbonaceous chondrite array. The vector of evaporation/condensation is also shown (dashed grey line) for a fractionation factor, $\Delta^{66}Zn_{liq\text{-}vap}$ = +1‰, with each value (grey circle) representing the fraction of Zn evaporated from a bulk Earth composition. The regression considers only carbonaceous chondrite analyses. The logarithmic scale on the abscissa means that the position of the Bulk Earth is relatively insensitive to the amount of Zn in the core.

Fig. 7. *[1 column]* The contrasting chemical signatures of nebular and post-nebular depletion in planetary materials. Carbonaceous chondrites (listed CI, CM, CV, and CO) show near-constant Mn/Na and decreasing δ^{66}Zn with progressive volatile depletion. The Earth lies at the volatile-poor end of this trend, whereas the Moon shows heavy δ^{66}Zn with respect to carbonaceous chondrites and markedly higher Mn/Na ratios. This latter trend is characteristic of volatile depletion under oxidising (post-nebular) conditions.

Fig. 8. *[1 column]* The contribution of 2-5 % CI chondrite or 5-15% CV chondrite during late accretion to the present-day element budget of the Earth's mantle. Ordinate values correspond to the fraction of the element in the

ACCEPTED MANUSCRIPT

proto-Earth prior to late chondrite addition, low values, as for Ag and Pb, indicate that most of their budget was delivered late. By contrast, CI- or CV addition is calculated to bring not more than 35% of the In, Zn, Rb and Mn, meaning the majority of the budget of these elements had to have been present in the proto-Earth prior to any late addition.

Acknowledgments

P.A.S. was supported by an Australian Postgraduate Award PhD Scholarship an ANU Vice-Chancellor's Scholarship and on the ERC grant Pristine. O.N. acknowledges support from FT140101062 and H.O'N. from Australian Research Council Discovery Grant DP130101355. F.M. is grateful to the European Research Council under the European Community's H2020 framework program/ERC grant agreement # 637503 (Pristine) and the Agence Nationale de la Recherche for a chaire d'Excellence Sorbonne Paris Cité (IDEX13C445), and for the UnivEarthS Labex program (ANR-10-LABX-0023 and ANR-11-IDEX-0005-02). We are grateful to the thorough reviews provided by two anonymous reviewers and Nadine Mattielli that honed the analytical descriptions, improved the framing of the question in a planetary context, and encouraged critical thinking of the causes of Zn isotope variability in the mantle. Parts of this work were supported by IPGP multidisciplinary program PARI, and by Region Île-de-France SESAME Grant no. 12015908

ACCEPTED MANUSCRIPT

ACCEPTED MANUSCRIPT

Table 1: Samples analysed for their Zn isotope composition in this work, classified by type; Peridotites and Pyroxenites from the Balmuccia massif, NW Italy, and a selection of global Komatiites, presented alongside some relevant geochemical data.

Sample	Locality	Class	Subclass	MgO (wt%)	FeO (wt%)	Zn (ppm)	δ^{66}Zn (‰)	2×St. Dev.	δ^{68}Zn (‰)	2×St. Dev.	n
Peridotites											
BM31	Balmuccia	Peridotite	Dunite	48.38	9.29	44.7	0.16	0.04	0.33	0.08	2
BM19	Balmuccia	Peridotite	Dunite	47.47	10.26	48.8	0.12	0.02	0.23	0.04	2
BD31	Balmuccia	Peridotite	Dunite	46.32	7.85	41.1	0.15	*0.06*	0.31	*0.12*	1
BM26B	Balmuccia	Peridotite	Depleted Lherzolite	43.30	8.04	52.1	0.11	*0.06*	0.60	*0.12*	1
BM42	Balmuccia	Peridotite	Depleted Lherzolite	42.15	8.11	46	0.16	*0.06*	0.30	*0.12*	1
BMH3-Pd	Balmuccia	Peridotite	Depleted Lherzolite	42.09	8.21	75.2	0.11	0.06	0.22	0.03	2
BM30	Balmuccia	Peridotite	Depleted Lherzolite	41.75	8.67	47.5	0.15	*0.06*	0.30	*0.12*	1
BMH-1	Balmuccia	Peridotite	Depleted Lherzolite	40.70	8.86	66	0.18	*0.06*	0.39	*0.12*	1
BMH-5	Balmuccia	Peridotite	Normal Lherzolite	40.10	8.09	46	0.12	*0.06*	0.25	*0.12*	1
BM35	Balmuccia	Peridotite	Normal Lherzolite	40.00	8.04	45	0.12	*0.06*	0.25	*0.12*	1
BM27	Balmuccia	Peridotite	Normal Lherzolite	39.81	8.30	52.9	0.14	0.04	0.28	0.09	2
BM40	Balmuccia	Peridotite	Normal Lherzolite	39.48	8.31	52	0.12	0.02	0.26	0.04	2
BM23	Balmuccia	Peridotite	Normal Lherzolite	39.35	8.31	43.5	0.14	0.02	0.29	0.15	2
BM29-Pd	Balmuccia	Peridotite	Enriched Lherzolite	39.20	8.24	43	0.10	*0.06*	0.20	*0.12*	1
BM12	Balmuccia	Peridotite	Normal Lherzolite	38.85	8.24	43.5	0.15	0.02	0.27	0.06	2
BM22	Balmuccia	Peridotite	Normal Lherzolite	38.77	8.22	47	0.18	0.06	0.37	0.08	2
BMH-9	Balmuccia	Peridotite	Normal Lherzolite	38.55	8.04	41.7	0.16	*0.06*	0.33	*0.12*	1
BMH-2	Balmuccia	Peridotite	Enriched Lherzolite	36.78	7.86	42	0.13	0.11	0.25	0.23	2
BM14	Balmuccia	Peridotite	Enriched Lherzolite	31.79	7.06	33.9	0.16	*0.06*	0.31	*0.12*	1
Pyroxenites											

ACCEPTED MANUSCRIPT

BM28-Px	Balmuccia	Pyroxenite	Chrome-Diopside	21.75	3.91	17	0.21	*0.06*	0.42	*0.12*	1
BMH3-Px	Balmuccia	Pyroxenite	Chrome-Diopside	19.96	4.00	52.1	0.23	0.01	0.45	0.01	2
BM29-Px	Balmuccia	Pyroxenite	Aluminium-Augite	18.48	5.00	70	0.18	*0.06*	0.37	*0.12*	1
Komatiites											
331/788	Barberton	Komatiite	Olivine Cumulate	43.69	5.44	22	0.04	0.01	0.10	0.04	2
176-725	Regal	Komatiite	Olivine Cumulate	35.13	10.88	54	0.16	*0.06*	0.33	*0.12*	1
422/86	Munro	Komatiite	Olivine Cumulate	32.45	8.60	60	0.20	*0.06*	0.41	*0.12*	1
422/84	Munro	Komatiite	Olivine Cumulate	28.50	9.21	57	0.16	*0.06*	0.33	*0.12*	1
422/84 (r)*	Munro	Komatiite	Olivine Cumulate	28.50	9.21	57	0.20	*0.06*	0.39	*0.12*	1
422/96*	Munro	Komatiite	Spinifex-Textured Komatiite	28.71	7.83	70	0.19	0.06	0.39	0.09	2
B-R1	Belingwe	Komatiite	Spinifex-Textured Komatiite	27.60	10.59	55	0.16	*0.06*	0.29	*0.12*	1
B-H2	Belingwe	Komatiite	Spinifex-Textured Komatiite	27.00	9.60	57	0.18	0.04	0.39	0.04	2
331/777a	Barberton	Komatiite	Spinifex-Textured Komatiite	25.10	11.17	68	0.19	*0.06*	0.38	*0.12*	1
331/779*	Barberton	Komatiite	Spinifex-Textured Komatiite	26.76	10.51	64	0.19	*0.06*	0.38	*0.12*	1
SD6/400*	Yilgarn	Komatiite	Spinifex-Textured Komatiite	27.99	10.34	71	0.20	*0.06*	0.40	*0.12*	1
179-755	Coonterunah	Komatiite	Spinifex-Textured Komatiite	24.32	9.32	58	0.16	0.02	0.36	0.11	2
179-751	Coonterunah	Komatiite	Spinifex-Textured Komatiite	23.33	10.69	139	0.20	*0.06*	0.40	*0.12*	1
331/778*	Barberton	Basalt	Spinifex-Textured Basalt	12.30	13.19	85	0.24	*0.06*	0.47	*0.12*	1
BR-S	Barberton	Basalt	Spinifex-Textured Basalt	13.84	9.17	62	0.20	*0.06*	0.40	*0.12*	1
RL-12-1	Red Lake	Basalt	Spinifex-Textured Basalt	13.68	10.83	63	0.22	*0.06*	0.43	*0.12*	1
RL-12-1 (r)*	Red Lake	Basalt	Spinifex-Textured Basalt	13.68	10.83	63	0.23	*0.06*	0.45	*0.12*	1
176-766	Coonterunah	Basalt	Spinifex-Textured Basalt	11.26	12.94	97	0.19	*0.06*	0.39	*0.12*	1
179/753	Coonterunah	Basalt	Basalt	4.05	13.39	178	0.22	0.01	0.43	0.02	2
Standards (This Work)											
JMC-LMTG	Zn Solution						-0.09	0.06	-0.18	0.10	3
BHVO-2	Kilauea	Basalt	Basalt	7.23	11.2	103	0.28	0.06	0.55	0.11	2

ACCEPTED MANUSCRIPT

Allende		Chondrite	CV3	24.59	30.32	110	0.21	0.04	0.41	0.10	2
PCC-1*	Cazadero	Peridotite	Serpentinised Harzburgite	43.43	7.91	42	0.27	0.08	0.53	0.14	2

* Denotes samples run at IPGP.

(r) denotes samples re-dissolved and processed.

Figures in italics denote external reproducibilities adopted from Sossi et al. (2015).

ACCEPTED MANUSCRIPT

ACCEPTED MANUSCRIPT

Table 2. Model parameters for the calculation of Zn isotope fractionation during non-modal partial melting of a fertile peridotite.

Phase	Starting fraction	Melting reaction[1]	Partitioning	D_{Zn}[2]	$\Delta^{66}Zn$ (‰)	T (K)
olivine	0.535	-0.25	ol/melt	0.96	$-0.17\times10^6/T^2$	
orthopyroxene	0.26	0.35	opx/melt	0.65	$-0.17\times10^6/T^2$	
clinopyroxene	0.185	0.80	cpx/melt	0.40	$-0.17\times10^6/T^2$	
spinel	0.02	0.10	sp/melt	5.20	$0\times10^6/T^2$	
Bulk	1	0	mantle/melt	0.86	$-0.15\times10^6/T^2$	1573

[1] Wasylenki et al. (2003)

[2]Le Roux et al. (2011); Davis et al. (2013).

ACCEPTED MANUSCRIPT

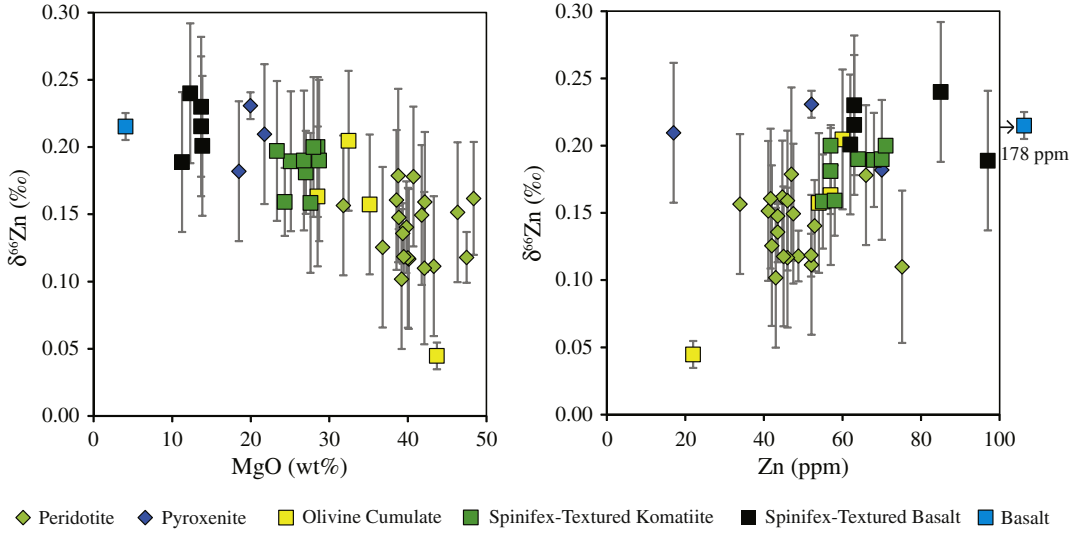
δ66Zn (‰)
MgO (wt%)
Zn (ppm)
178 ppm
Peridotite
Pyroxenite
Olivine Cumulate
Spinifex-Textured Komatiite
Spinifex-Textured Basalt
Basalt

Figure 1

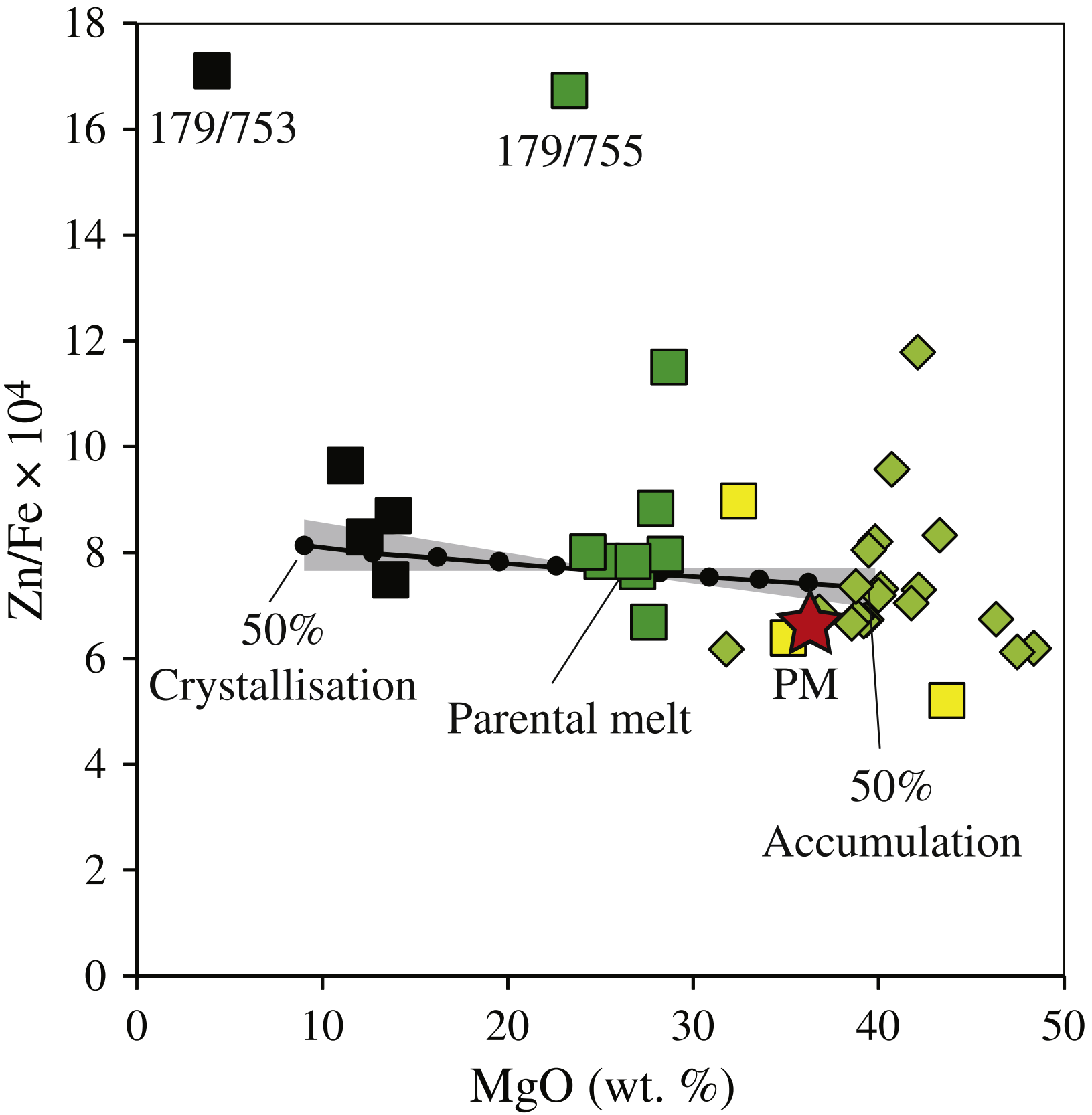
18
16
14
12
10
8
6
4
2
0
Zn/Fe × 10⁴
179/753
179/755
50%
Crystallisation
Parental melt
PM
50%
Accumulation
0
10
20
30
40
50
MgO (wt. %)

Figure 2

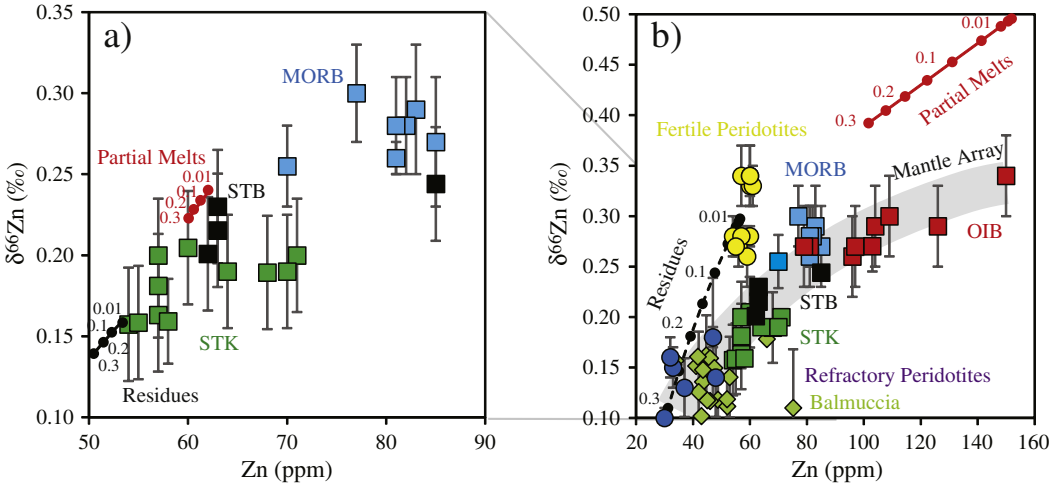
a)
b)
δ66Zn (‰)
Zn (ppm)
MORB
Partial Melts
STB
STK
Residues
Fertile Peridotites
Mantle Array
OIB
Refractory Peridotites
Balmuccia
0.01
0.1
0.2
0.3

Figure 3

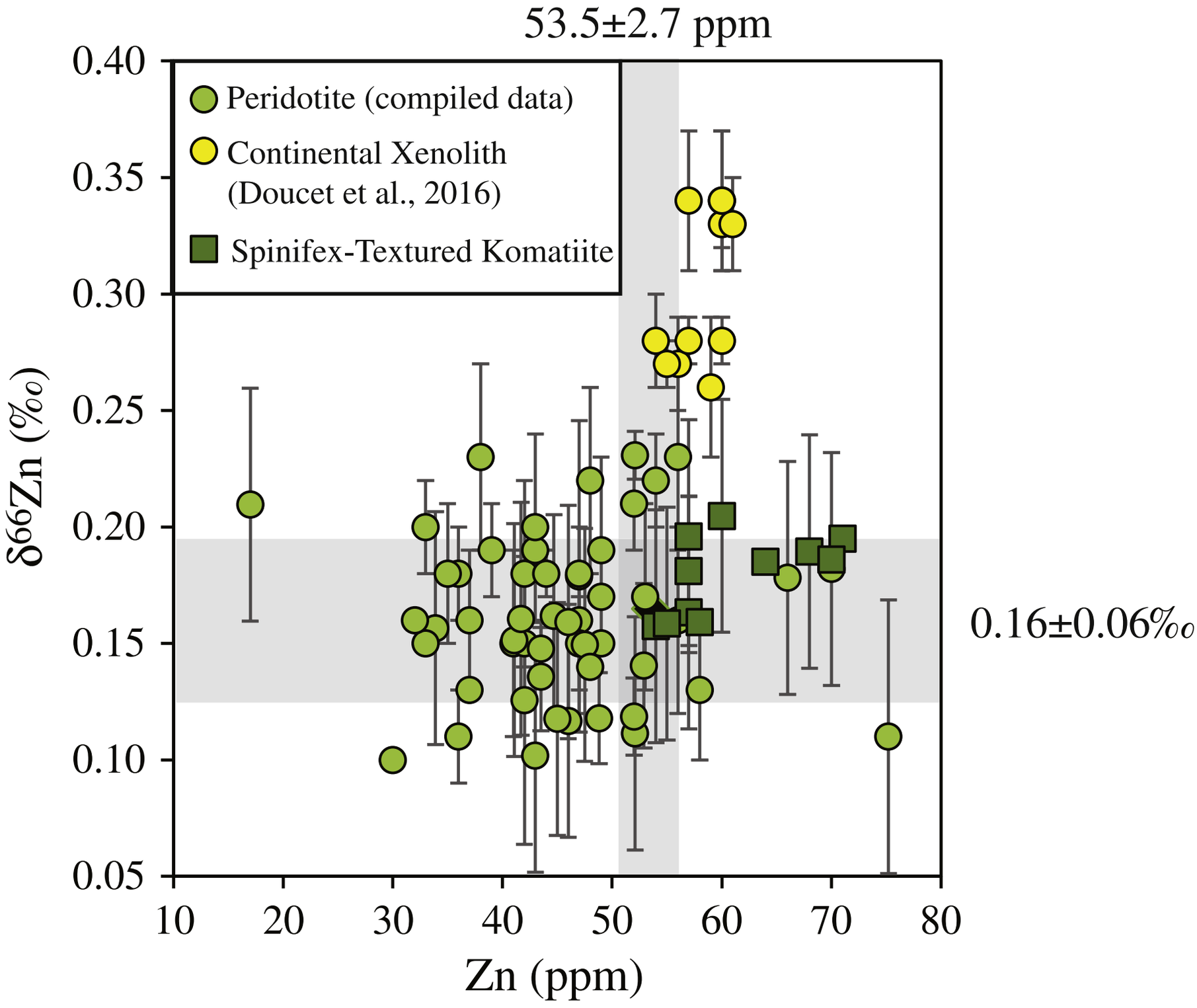
53.5±2.7 ppm
Peridotite (compiled data)
Continental Xenolith
(Doucet et al., 2016)
Spinifex-Textured Komatiite
0.16±0.06‰
δ66Zn (‰)
Zn (ppm)
0.40
0.35
0.30
0.25
0.20
0.15
0.10
0.05
10
20
30
40
50
60
70
80

Figure 4

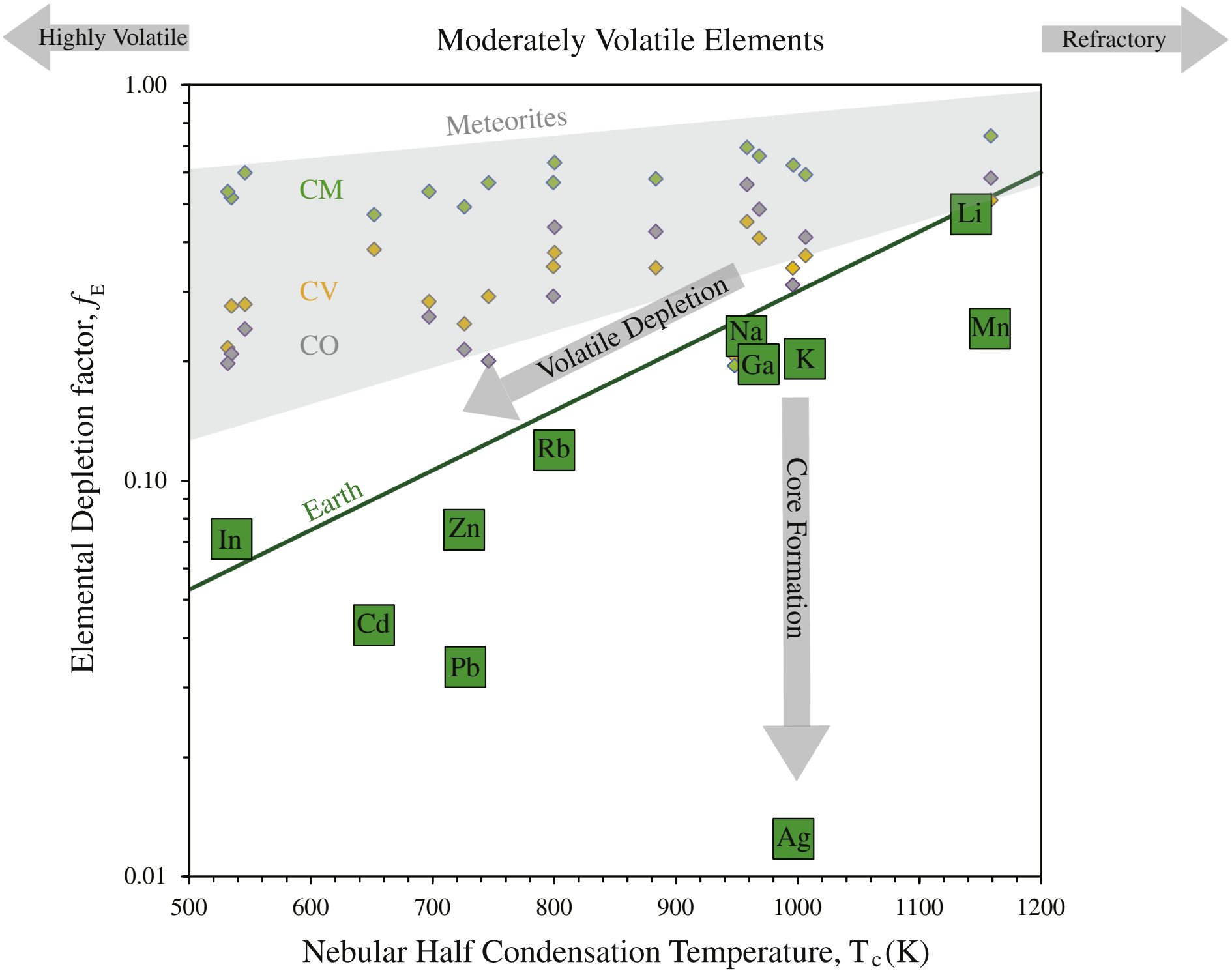
Highly Volatile
Moderately Volatile Elements
Refractory
1.00
0.10
0.01
Elemental Depletion factor, f_E
Meteorites
CM
CV
CO
Volatile Depletion
Earth
Core Formation
Li
Mn
Na
Ga
K
Rb
In
Zn
Cd
Pb
Ag
500
600
700
800
900
1000
1100
1200
Nebular Half Condensation Temperature, T_c (K)

Figure 5

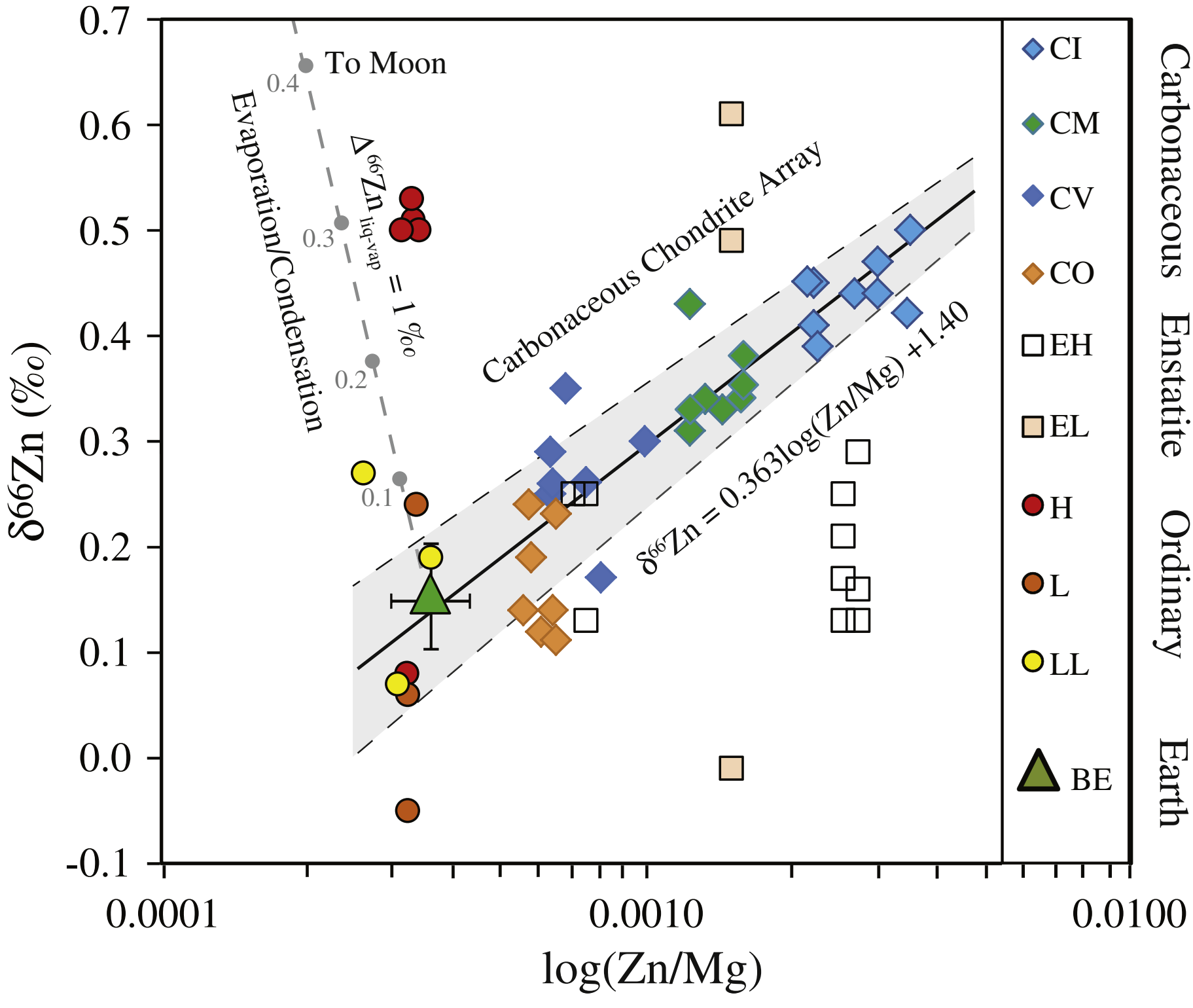
0.7
0.6
0.5
0.4
0.3
0.2
0.1
0.0
-0.1
δ66Zn (‰)
0.0001
0.0010
0.0100
log(Zn/Mg)
To Moon
0.4
0.3
0.2
0.1
Evaporation/Condensation
Δ66Zn liq-vap = 1 ‰
Carbonaceous Chondrite Array
δ66Zn = 0.363log(Zn/Mg) +1.40
CI
CM
CV
CO
EH
EL
H
L
LL
BE
Carbonaceous
Enstatite
Ordinary
Earth

Figure 6

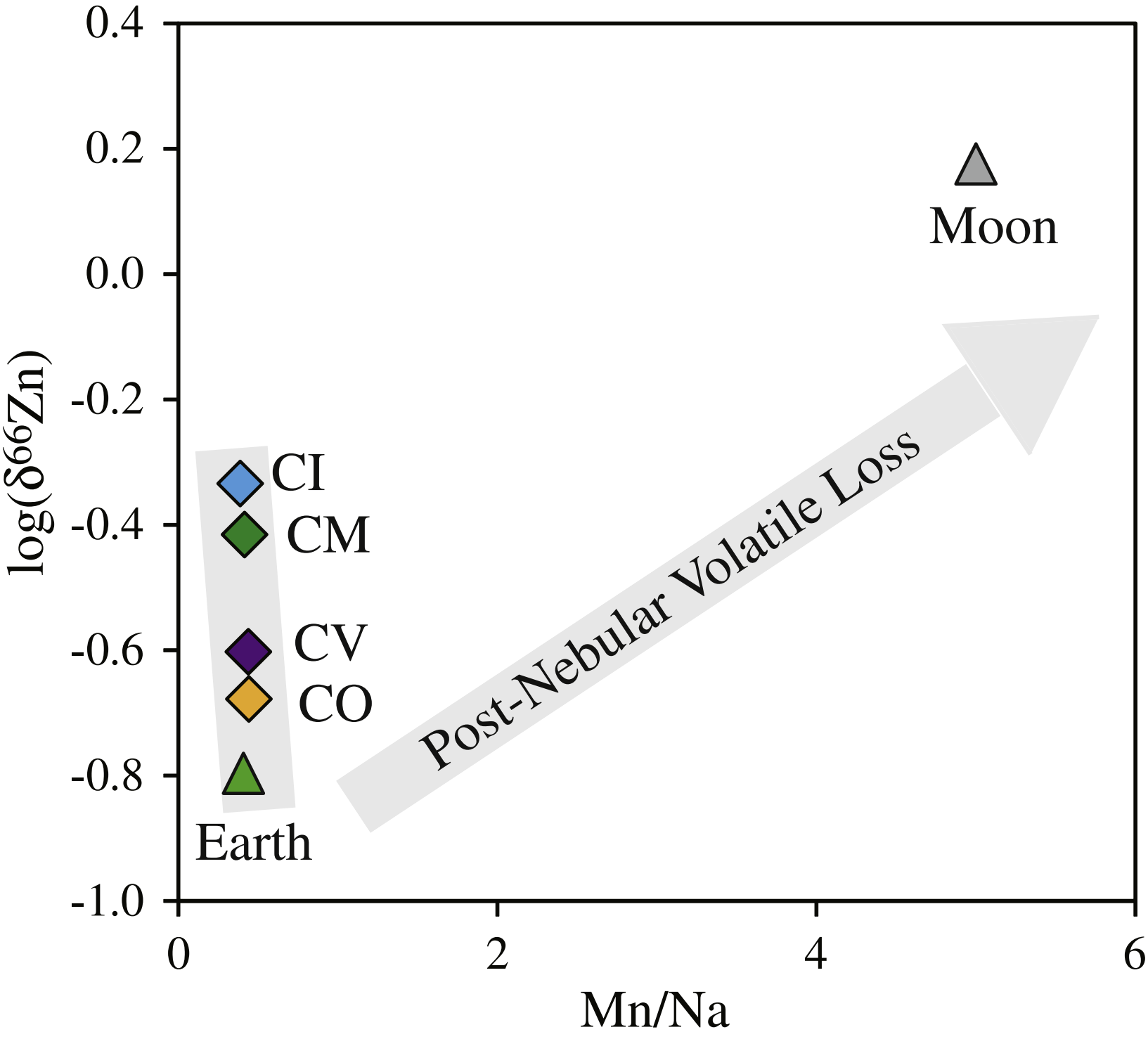
0.4
0.2
0.0
-0.2
-0.4
-0.6
-0.8
-1.0
log(δ66Zn)
0
2
4
6
Mn/Na
Moon
CI
CM
CV
CO
Earth
Post-Nebular Volatile Loss

Figure 7

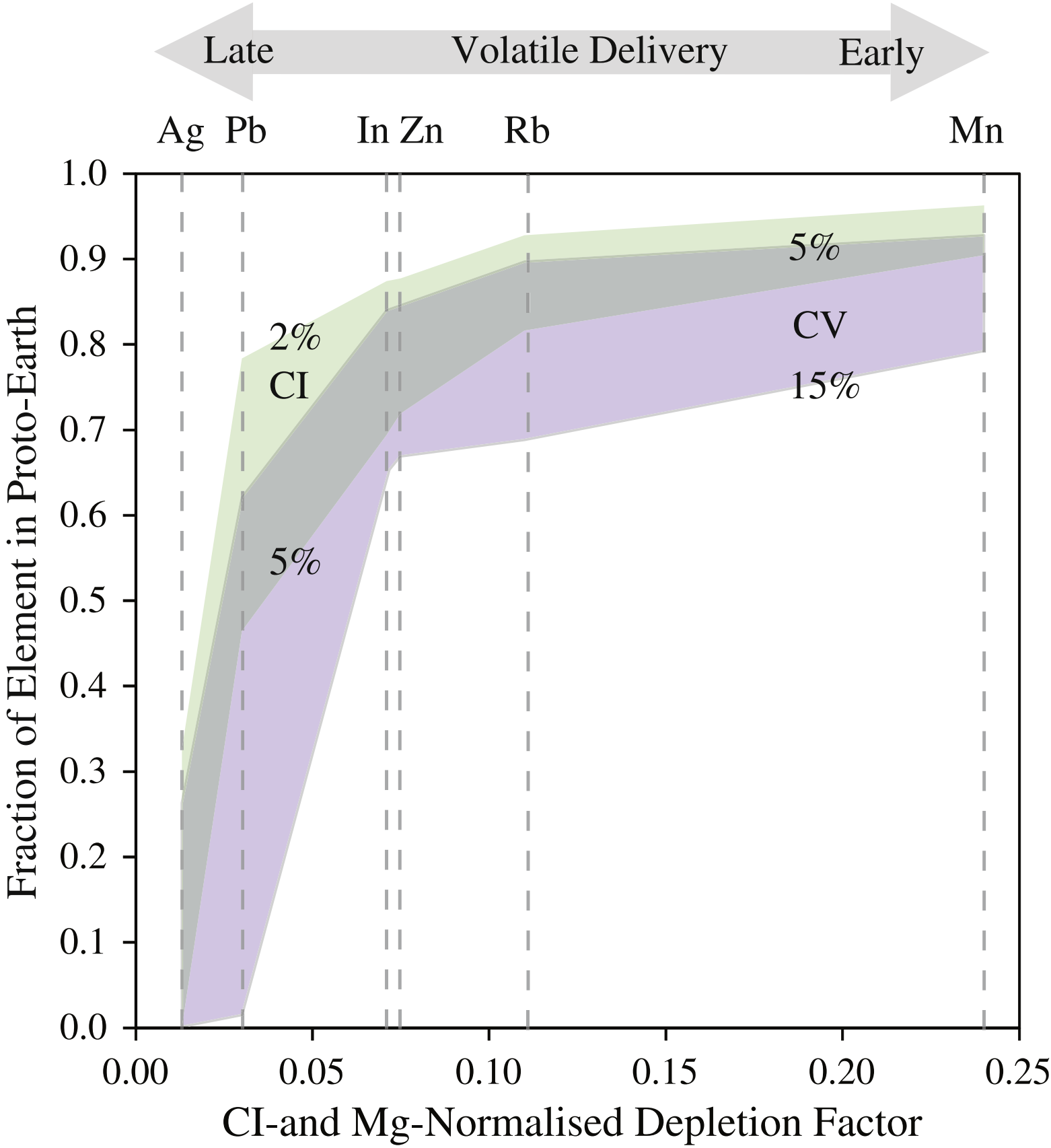
Late
Volatile Delivery
Early
Ag
Pb
In
Zn
Rb
Mn
1.0
0.9
0.8
0.7
0.6
0.5
0.4
0.3
0.2
0.1
0.0
Fraction of Element in Proto-Earth
2%
CI
5%
5%
CV
15%
0.00
0.05
0.10
0.15
0.20
0.25
CI-and Mg-Normalised Depletion Factor

Figure 8